J. Fluid Mech. (1979), *vol.* 91, *part* 4, *pp.* 731–763
Printed in Great Britain

A vortex theory of animal flight. Part 2. The forward flight of birds

By J. M. V. RAYNER

Department of Applied Mathematics and Theoretical Physics, University of Cambridge†

(Received 18 May 1978)

The vortex wake of a bird in steady forward flight is modelled by a chain of elliptical vortex rings, each generated by a single downstroke. The shape and inclination of each ring are determined by the downstroke geometry, and the size of each ring by the wing circulation; the momentum of the ring must overcome parasitic and profile drags and the bird's weight for the duration of a stroke period. From the equation of motion it is possible to determine exactly the kinematics of the wing-stroke for any flight velocity. This approach agrees more readily with the nature of the wing-stroke than the classical actuator disk and momentum-jet theory; it also dispenses with lift and induced drag coefficients and is not bound by the constraints of steady-state aerodynamics. The induced power is calculated as the mean rate of increase of wake kinetic energy. The remaining components of the flight power (parasite and profile) are calculated by traditional methods; there is some consideration of different representations of body parasite drag. The lift coefficient required for flight is also calculated; for virtually all birds the lift coefficient in slow flight and hovering is too large to be consistent with steady-state aerodynamics.

A bird is concerned largely to reduce its power consumption on all but the shortest flights. The model suggests that there are a number of ways in which power reduction can be achieved. These various strategies are in good agreement with observation.

1. Introduction and outline of the model

The theory described in this paper is an attempt to find a more rigorous physical background to the problem of the steady forward flight of birds than has been available in previous work on the subject. It provides realistic estimates of power consumption and of mean lift coefficients by assuming that the wake consists of a sequence of disjoint plane elliptic vortex rings. Power consumption is of interest as it is one of the main factors involved in the choice of a particular flight strategy or 'style'; reduction of power is of great concern to a bird on long (e.g. migratory) flights. The mean lift coefficient indicates to what extent we can expect steady or quasi-steady aerodynamics to apply to the whole wing. Existing theories depend on steady-state analysis and are unsatisfactory, especially at low velocities, and it is the need to overcome this difficulty that has been the main inspiration for this theory.

Flight is one of many responses to evolutionary stimulus found in the animal kingdom; it allows great flexibility in habits and habitat and requires a simple locomotor system in which only one set of organs, the wings, generates all of the forces required. In this respect all flying animals are similar, but the method by which flight is achieved

† Present address: Department of Zoology, University of Bristol.

0022-1120/79/4171-6260 $02.00 © 1979 Cambridge University Press

varies greatly between birds and insects; we are concerned here solely with birds, and make only passing reference to insects and bats. We neglect the hummingbirds (*Trochili*), whose flight behaviour is more akin to that of the insects.

The aerodynamic aspects of animal flight are of great interest to ornithologists and physicists alike, but the topic is complex and must be simplified before any progress can be made. The goal of most such studies is the estimation from theoretical arguments of power consumption under various flight conditions, which can be compared with physiological measurements. Power is important as it indicates the rate at which fuel reserves are used up, and the rate at which chemical energy is converted into mechanical work by the muscles. Both of these are limited, and form a major constraint on flight capability.

We must isolate the most important dimensions of the body (morphologic parameters) and characteristics of the wing-stroke (kinematic parameters) during flight. The morphologic parameters we use are the mass M, wing semi-span b (assumed equal to the wing length), wing chord, c_0, wing area (both wings) S, and the masses m_s and m_p of the two pairs of muscles powering the up- and downstrokes. (For most birds m_s is about one-tenth of m_p.) The kinematic parameters can be reduced to four. The most important is the stroke period T, which depends on body size; its measurement is fraught with difficulties; the problems involved are discussed in Rayner (1979*b*, §5). Associated with T are the downstroke ratio τ (so that τT is the duration of the downstroke) and the beat amplitude ϕ. Typically τ is about $\frac{1}{2}$ or slightly less and ϕ is between 80 and 120°, rising to nearly 180° during hovering in some instances. The remaining parameter is the stroke-plane angle γ. We assume that the leading edges of the wings remain in the same plane throughout the downstroke; γ is the angle between this plane and the horizontal.

The relative magnitude and durations of the different phases of the wing-stroke as characterized (at least, simplified) by the kinematic parameters together with the morphologic parameters for a particular bird enable us to define and quantify 'flight style'. Flight style is a term introduced to describe the pattern of flight adopted by an individual or a group from a particular species. We can assume that the style chosen carries distinct advantages, either aerodynamic, physiological, anatomical or simply behavioural, and that the range of kinematic and morphological parameters available is associated with the choice of style. This could be manifest as a preference for flying in a flock or in the V-shaped pattern typical of migrating geese; it might lead to gliding or soaring, especially if the animal is large, or to a combination of gliding with intermittent bursts of wing flaps (undulating flight). Many small birds can save energy by using bounding flight (Rayner 1977, 1979*b*, §§4 and 5); the majority of species will spend some of their time in the air in steady level flight, and it is here that the morphology will dictate, as a means of saving energy or of relaxing the structural or physiological constraints which limit flight, the choice of kinematic parameters and hence of flight style.

In some species the flight style depends upon the flight velocity, and we divide the speed range broadly into two parts. Fast forward flight is the normal cruising mode; the wing always has some component of forward velocity and the beat amplitudes are small. In slow forward flight the wing-beats are generally of larger amplitude with the tips coming to rest at the extremes of the stroke. Oehme (1968) found discontinuities in both the wing-beat amplitude and the period at the transition from slow to

fast flight in the swift, and Oehme & Kitzler (1975*b*) noted that in fast forward flight of the pigeon τ increases and ϕ decreases with increasing flight speed. Hovering can be considered to be the lower limit of slow forward flight; not all birds are able to hover because of the high energy cost and the difficulty of obtaining sufficient lift; there is a marked drop in power as the forward velocity increases from hovering.

In the previous part of this paper (Rayner 1979*a*, referred to as I) a detailed application of the vortex theory to animal hovering was given. Many of the arguments given in I, § 1, are equally relevant to forward flight and need only be summarized here. Paper I discussed solely the induced power, since in hovering the other power components are easy to calculate; here, a largely similar technique is used for the induced power, but careful consideration is given also to the drag forces on the body, which influence the strength and inclination of the wake momentum required for propulsion and lift. To give a true picture of the total power consumed in forward flight we also calculate the rate of working required to overcome parasite and profile drags. A further paper (Rayner 1979*b*) gives a less mathematical version of the theory given in I and here, together with some of the biological deductions which we may make.

The usual method of calculating the induced power is the Rankine–Froude momentum jet produced by an actuator disk (I, § 2). The most obvious fault of this approach is its assumption that momentum is generated steadily, clearly untenable in animal flight. In hovering it is conceptually straightforward to imagine the vortex sheet forming the boundary of the jet to be broken up into discrete elements, which we represent in I as small-cored circular vortex rings. In forward flight the procedure we should use is not evident, since the wake momentum cannot be parallel to the wake itself, and it is difficult to see how we should define the actuator disk (e.g. what size and inclination it should have). However, it is clear that a trailing vortex sheet is formed behind the wings during each downstroke, and we seek a simple geometric representation for the final form of this sheet.

In avian flight the upstroke is typically very lightly loaded, and has relatively little aerodynamic effect. This implies that the vortex element produced by each downstroke is distinct from its neighbours; at high flight velocities the elements are well spaced and interaction between them is minimal. Provided that we can find a suitable geometry for the wake elements, the induced power can be calculated as the rate of supply of kinetic energy to the flows induced in the wake by vorticity.

The trailing vortex sheet is a complicated, twisted structure; its boundary is defined by the wing-tip paths and its ends by the starting and stopping vortices formed at the beginning and end of each stroke. It contains vorticity both parallel and transverse to the direction of flight, and is deforming continuously. Evidently it would be a major problem to trace the evolution of such a vortex sheet. However, according to the arguments given in I, § 1, and expanded in Rayner (1979*b*, § 3), we can expect the sheet to roll up into a closed vortex loop of small core cross-section, and with the same impulse and energy as the sheet provided that the roll-up occurs rapidly. We must assume that this is so, and that no destructive instability operates within the time scale of the wing beat. It seems reasonable, as an extension of the arguments given in I, § 1, that the resulting vortex loop should be elliptic in shape (see figure 3), tilted with respect to the flight direction in order that there is a forward component

of momentum, and with dimensions proportional to the wing-span and to the distance between the positions of the wing tips at the start and finish of the downstroke. The constant of proportionality will (as in I, §5) depend upon the circulation distribution on the wing. We base the forward-flight model on the assumption that this is the shape of each wake element, at least for the time after generation during which the element can have any effect on the power requirement.

There is some evidence that vortex rings are the mechanism by which wake momentum is generated, although there is no information about their shape. Ellington (1978) has shown that vortex loops are the mechanism of insect hovering; we argue in I, §3 that while stroke kinematics differ between birds and insects the wakes are similar, and that we can expect vortex rings in avian hovering. Magnan, Perrilliat-Botonet & Girard (1938) photographed a sequence of closed vortices behind a pigeon in very slow flight; Pennycuick & Lock (1976) give an argument based on feather deformation which suggests (indirectly) how vortices are shed by the downstroke.

To obtain the wake kinetic energy, and hence the induced power, we need expressions for the self-induced velocity and energy of an isolated small-cored elliptic vortex loop; these are derived in the appendix.

The model is in outline an extension of that given by Pennycuick (1968, 1969), but by comparison offers a wider range of input parameters, more exact calculation of the profile power and the nature of the induced forces, and most important, a more satisfactory description of the wake. Pennycuick's theory has been modified by Tucker (1972, 1973); the various versions have been summarized by Pennycuick (1975), and the biological implications in some detail by Oehme, Dathe & Kitzler (1977). Although it is the most widely used flight power theory, Pennycuick's is not the only one available; a similar but less satisfactory model again based on the momentum jet, but omitting profile drag, has been given by Greenewalt (1975). In addition, various earlier theories are summarized by Brown (1963). Osborne (1951) and Weis-Fogh (1972, 1973), both concerned with insect flight, have prompted the method of calculation of profile drag and mean lift coefficients we use.

Among over valuable studies of flight are reviews by Lighthill (1974) and Nachtigall (1974). Detailed descriptions of wing motions are given in Brown (1963) and Bilo (1971, 1972), and many fine photographs will be found in Rüppell (1977). Cone (1968) attempts to set up a vortex theory of flapping flight, which becomes too complicated to be solvable. It is assumed that the reader is familiar with the essentials of avian anatomy and with the nature of the wing-stroke. These are widely described in the literature; among the more useful discussions, in addition to those above, is George & Berger (1966).

2. Power components

The analysis of the active flight of birds (and insects) is a problem in unsteady aerodynamics of extreme complexity. We have little information about the air flow near to the animal's body and wings, and cannot hope to obtain this by the usual aerodynamic techniques. The impulse method, applied to a vortex wake, allows us to deduce the power consumed. This method is classically concerned with the dynamics of a fixed-wing aircraft, where the wings are responsible for lift and thrust is obtained from essentially separate propellers or jets. In a helicopter there is more similarity

with natural flight as the rotor blades generate both lift and thrust, but it is difficult to relate helicopter geometry to a bird or insect in forward flight. An almost universal property of flying animals is that the same pair of organs, the wings, are responsible for both lift and thrust, and that all of the energy required for flight must be provided by the locomotor muscles. In some species of bird the tail and feet can provide some additional lift, but their more usual function is to assist with stability and to increase drag while landing or decelerating. Body drag is sizeable, and the body can also contribute to lift (Csicsáky 1977).

Flight-power consumption and metabolic power supply are major factors dictating an animal's flight proficiency, in much the same way that the equivalent criteria are critical for an aircraft. For an aircraft the power required for steady level flight can be divided into three components:

P_{par}, parasite power to overcome body drag;

P_{pro}, profile power to overcome wing form and friction drag;

P_i, induced power to overcome the induced drag of the wings.

In level flight the angle of attack of the wings is adjusted such that lift balances the weight, and engine thrust is altered independently to balance the total drag. The aerodynamic characteristics of an aircraft are well known in terms of force coefficients, and the power components may be readily evaluated.

A similar framework is suitable to describe animal flight. The parasite and profile powers again measure the work rate overcoming body and wing drags, but the induced power cannot be conceived as the rate of working against induced drag since the formulation of induced drag in terms of lift and drag coefficients is not consistent with unsteady aerodynamics, which we know must apply at least at low flight velocities. The novel approach used here is to calculate the induced power as the rate at which kinetic energy is supplied to vortex-induced flows in the wake whose momentum provides lift and thrust. The energy expended against profile and parasite drags passes to a viscous wake which we assume to be independent from the 'useful' vortex wake.

In addition to the parasite, profile and induced powers we might also include the energy lost in decelerating the wings at the end of the downstroke (which becomes inertial power). Weis-Fogh (1973) has shown that this is significant for insects in hovering; because of the different scales involved it is not likely to contribute significantly in a bird's energy budget, and we neglect it here.

The vortex sheet shed during each downstroke is assumed to become a plane elliptic vortex ring of small core radius (see Rayner 1979*b*, §3), with appropriate dimensions and orientation; each ring must support the bird's weight and overcome profile and parasite drags for the duration T of the stroke cycle. Successive rings are separated by self-convection and by the distance travelled by the bird in a time T; the configuration is illustrated in figure 3. The induced power is calculated as the increment in wake kinetic energy on the addition of a further member to the chain of vortices (assumed semi-infinite) formed by preceding wing-strokes.

Our procedure is to assume that the kinematic parameters ϕ, τ and T are fixed, and to set up the equations for the balance of the forces on the animal as a function of the stroke-plane angle γ for a forward velocity V. With the addition of a simple

description of the mechanism of formation of each vortex ring we can solve these equations to obtain $\gamma(V)$, and hence find the power components as functions of V.

3. Forces on the body

We assume that throughout each downstroke the leading edges of the wings remain in a plane relative to the bird which is inclined to the horizontal at an angle γ and that during each upstroke the wing is flexed to minimize aerodynamic resistance. The notation is indicated in figures 1 (*a*) and (*b*). The angular position of the wing is given by $\theta(t)$ $(0 < t < \tau T)$ and radial position on a wing by $b\zeta$ $(0 < \zeta < 1)$. The left and right wings are denoted by $\pm$ signs, respectively. The wing chord is given by $c_0\bar{c}(\zeta)$, where $\bar{c}(0) = 1$. Oehme & Kitzler (1975*a*) have shown that bird wings in general conform closely to the shape

$$\bar{c}(\zeta) = \begin{cases} 1 & \text{for} \quad 0 < \zeta < \frac{1}{2}, & (1a) \\ 4\zeta(1-\zeta) & \text{for} \quad \frac{1}{2} < \zeta < 1; & (1b) \end{cases}$$

we use this expression throughout. The bird's weight is given by $-Mg\mathbf{k}$.

The drag forces acting on the bird are the parasite drag of the body and the resultant of the profile drag of the wings. We consider first the parasite drag $\mathbf{D}_{\text{par}}$. This is the force on the body due to its resistance to the free air stream and to the induced flows generated by the wing motions; the induced contribution is very small and will be neglected. In the same way we neglect any drag caused by wing/body interactions as small.

There is some doubt about the value which should be assigned to the parasite drag. It can be assumed to be of the form

$$\mathbf{D}_{\text{par}} = \tfrac{1}{2}\rho\mathbf{A}_{fp}\,V^2, \tag{2}$$

where the vector $\mathbf{A}_{fp}$, which has the dimensions of area, is independent of V. Its components are the 'equivalent flat-plate areas' of the body for flow in the appropriate direction; they are considerably smaller than the body surface area, since the body is well streamlined. If the body is inclined above the free air stream there is likely to be a significant contribution to lift, but of the various published measurements of drag only one set takes account of this complication. The air density is given by ρ.

Difficulties in assigning a value to $\mathbf{A}_{fp}$ can arise in two ways. First, measurements on real birds are difficult to make, and are hence very scanty and not necessarily reliable; with the available data it is not easy to make a good estimate of the drag for an arbitrary bird, since there is a good deal of variation in body proportions over the size range. Second, and more serious, the body configuration of any individual will vary with the flight configuration, and we shall see that this can have an important effect on both drag and lift; it is difficult to apply any mathematical specification to the behaviour of body tilting since there is very little discussion of the problem in the literature. A third complication is the possible influence of the Reynolds number *Re*, but in the size range of avian flight this should not greatly influence the drag coefficients; despite overestimates of the influence of certain parameters Greenewalt (1975) has shown that variations in *Re* do not greatly alter our conclusions on power consumption.

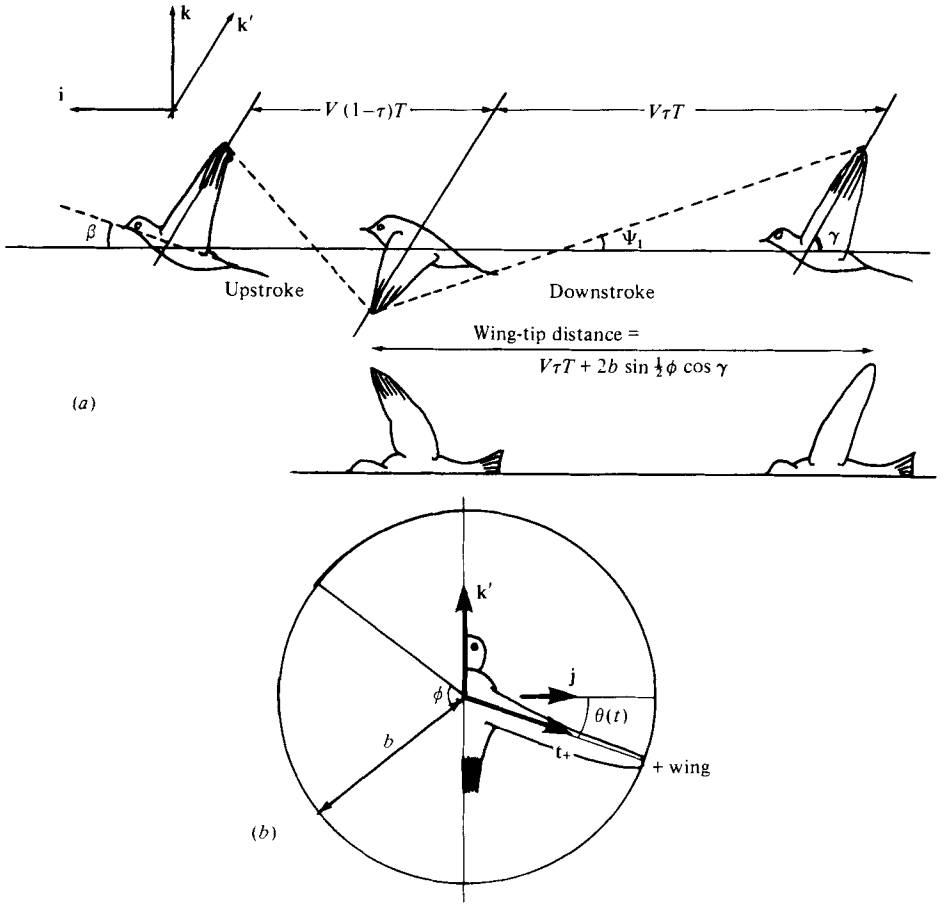

FIGURE 1. (*a*) One complete wing-beat in forward flight, showing notation used in power calculations. Flight velocity $\mathbf{V} = V\mathbf{i}$. The configuration of kinematic parameters is approximately consistent with a pigeon flying at 9 m s^{-1} (viz. $\gamma \approx 75°$, $\phi \approx 90°$, $\tau \approx \frac{4}{7}$). The unit vectors $\mathbf{j}$ (not shown) $= -\mathbf{i} \wedge \mathbf{k}$ and $\mathbf{k}'$ lie in the stroke plane. (*b*) Front view of bird in stroke plane ($\mathbf{j}$, $\mathbf{k}'$). Angular position of wing relative to horizontal (mid-stroke) is given by $\theta(t)$.

To simplify the effect of dimensional scaling, we assume that $|\mathbf{A}_{fp}|$ is proportional to (body mass)$^{\frac{2}{3}}$. Until more measurements are available we cannot predict the index any more accurately. From measurements on the pigeon, Pennycuick (1968) found

$$\mathbf{A}_{fp} = -2{\cdot}85 \times 10^{-3} M^{\frac{2}{3}} \mathbf{i} \quad (\mathrm{m}^2), \tag{3}$$

assuming that the body occupied the zero-lift configuration throughout. By including measurements from seven species and, like Pennycuick, assuming that the body is untilted, Tucker (1973) gives

$$\mathbf{A}_{fp} = -3{\cdot}34 \times 10^{-3} M^{\frac{2}{3}} \mathbf{i} \quad (\mathrm{m}^2), \tag{4}$$

somewhat greater than Pennycuick's estimate. It is reasonable to expect (4) to apply in fast forward flight, but in slow forward flight and hovering the body is tilted by angles of up to about 45°. An estimate of the effect of this can be made by assuming that the equivalent flat plate area for the drag component normal to the body is the same as the projected area of the body A_b, with the drag parallel to the axis of the

body as in (4). Then if the body axis is inclined at an angle β to the forward direction

$$\mathbf{A}_{fp} = -\mathbf{i}(A_f \cos^3\beta + A_b \sin^3\beta) + \mathbf{k}(A_b \sin\beta - A_f \cos\beta)\sin\beta\cos\beta, \tag{5}$$

where

$$A_f = 3{\cdot}34 \times 10^{-3} M^{\frac{2}{3}} \quad (\mathrm{m}^2). \tag{6}$$

Measurements by the author on a pigeon of mass 0·37 kg give $A_b = 0{\cdot}027$, compared with $A_f = 0{\cdot}0017$. Assuming that A_b scales as $M^{\frac{2}{3}}$, we calculate the scaling formula

$$A_b = 4{\cdot}5 \times 10^{-2} M^{\frac{2}{3}} \quad (\mathrm{m}^2). \tag{7}$$

It is unreasonable to claim this scaling on the basis of just one measurement, but as an indication of the order of magnitude of the lift obtained when the body is tilted it is valuable.

The only measurements available for the drag of a tilted body are those of Csicsáky (1977), who used plaster models of the zebra finch in observed body configurations. He obtained the drag and lift as functions very similar in behaviour to (5), but with magnitude $\frac{1}{3}$ or $\frac{1}{2}$ of that suggested by (6) and (7). Some of the discrepancy might be explicable by better streamlining in the finch than the pigeon, but most is probably due to his use of models, the smooth surface of which cannot compare with the birds' feathers. We cannot expect these measurements to confirm the estimates of (6) and (7), but they do suggest that the form of the expression in (5) is appropriate. Csicsáky gives figures which allow us to derive the following expression for $\mathbf{A}_{fp}$:

$$\mathbf{A}_{fp} = [-\mathbf{i}(1{\cdot}142 + 7{\cdot}141(\beta - \beta_0)^{2{\cdot}434}) + \mathbf{k}(7{\cdot}486(\beta - \beta_0)^{1{\cdot}405})]\, M^{\frac{2}{3}} \times 10^{-3} \quad (\mathrm{m}^2), \tag{8}$$

where $\beta_0 = \frac{1}{36}\pi\,(= 5°)$, β and β_0 being expressed in radians.

Assuming that we accept either of the representations (5) [with (6) and (7)] or (8) for $\mathbf{A}_{fp}$, we must specify how β behaves, either as a function of the flight velocity or, and more sensibly, as a function of the stroke-plane angle γ (angle of stroke plane to backwards direction $-\mathbf{i}$). In fast forward flight we expect β to be small and γ large, but the problem of relating them depends on the flexibility of the system of bones and muscles around the humeral joint. If the joint were totally inflexible we might suggest

$$\beta = 80° - \gamma, \tag{9}$$

but such a relation would lead to abnormally high values of β in slow flight, where γ is reduced more substantially than β is increased. Alternatively we might suggest that there is some value of $\beta + \gamma$ beyond which the anatomy cannot stretch, so that, say,

$$\beta = \max(\beta_1 - \gamma, 0), \tag{10}$$

where β_1 might lie between 35 and 80°. While such a relation is quite feasible and agrees well with known behaviour, we can expect β_1 to depend upon the species of bird involved, and to have a decisive effect upon flight style, so that a determined estimate for all species is not reasonable. Csicsáky quotes $\beta_1 = 55°$ for the zebra finch.

We experiment with a number of forms of the relation between β and γ together with different forms and magnitudes of $\mathbf{A}_{fp}$.

The parasite drag and the weight are important forces acting on the bird, but we must also consider the reaction of the wing motions. These are not constant through the stroke and would lead to recoil of the body, but we assume that the animal is

sufficiently massive for this to be neglected. The force on the body due to profile drag is small, but can be important at high velocity. The reaction of wing inertia is large during the downstroke, but its net effect is zero, so it can be ignored.

We calculate the profile drag (and later the profile power and lift coefficients) by a method derived from that of Osborne (1951), Pennycuick (1968) and Weis-Fogh (1972). Pennycuick included induced drag in the profile-drag calculation and thus seriously overestimated the profile power at low speeds; Weis-Fogh was concerned with hovering alone. We need to estimate a zero-lift drag coefficient C_{D0} for the wings; a value of 0·02 seems to be a good, if slightly large, estimate for bird wings; higher values are appropriate for insects. This coefficient represents the friction and form drags of the wing when producing zero lift; this formulation allows us to neglect the deformation of wing sections under aerodynamic load as a device to generate and retain wing circulation whose energy cost is included in the induced power. The reaction of the lift and induced drag forces is the momentum of the shed vortex sheet, which must be in equilibrium with the other forces acting on the body.

We define the origin of the coordinate axes as the initial position of the humeral joint (see figures 1*a*, *b* for notation). The angular velocity of the wing can be taken as sinusoidal during the downstroke (Norberg 1975), so that the angular position is given for $0 < t < \tau T$ by

$$\theta(t) = -\tfrac{1}{2}\phi \cos\frac{\pi t}{\tau T}, \tag{11}$$

and the angular velocity by

$$\dot{\theta}(t) = \tfrac{1}{2}\frac{\pi\phi}{\tau T}\sin\frac{\pi t}{\tau T}. \tag{12}$$

The position $\mathbf{X}_\pm$ of a point at radius ζ on the $\pm$ wing is given by

$$\mathbf{X}_\pm = Vt\mathbf{i} \pm b\zeta\mathbf{j}\cos\theta - b\zeta\mathbf{k}'\sin\theta; \tag{13}$$

the velocity of a wing section relative to the air is

$$\mathbf{U}_\pm = V\mathbf{i} - b\zeta\dot{\theta}(\pm\mathbf{j}\sin\theta + \mathbf{k}'\cos\theta), \tag{14}$$

with magnitude

$$U = (V^2 + 2Vb\zeta\dot{\theta}(t)\cos\theta\cos\gamma + b^2\zeta^2\dot{\theta}^2)^{\frac{1}{2}}. \tag{15}$$

For convenience we non-dimensionalize time with respect to the downstroke period divided by π, and velocity by the mean downstroke tip velocity times $\frac{1}{2}\pi$, writing

$$\bar{t} = \pi t/\tau T, \quad \bar{V} = 2V\tau T/b\phi\pi. \tag{16), (17}$$

The profile force per unit length on a wing section is

$$\mathbf{F}_{\mathrm{pro}\pm} = -\tfrac{1}{2}\rho c_0\bar{c}(\zeta)C_{D0}U\mathbf{U}_\pm, \tag{18}$$

so that the mean profile drag acting on the body,

$$\mathbf{D}_{\mathrm{pro}} = -\frac{b}{T}\int_0^{\tau T} dt \int_0^1 d\zeta\,(\mathbf{F}_{\mathrm{pro}_+} + \mathbf{F}_{\mathrm{pro}_-}), \tag{19}$$

can be expressed as

$$\mathbf{D}_{\mathrm{pro}} = \tfrac{1}{4}\pi\frac{\rho b^3 c_0 C_{D0}\phi^2}{\tau T^2}\int_0^1 d\zeta\int_0^\pi d\bar{t}\,\bar{c}(\zeta)\,\overline{U}(\zeta,t)\{\bar{V}\mathbf{i} - \zeta\sin\bar{t}\cos(\tfrac{1}{2}\phi\cos\bar{t})\,\mathbf{k}'\}, \tag{20}$$

where

$$\overline{U} = (\bar{V}^2 + 2\bar{V}\zeta\cos\gamma\sin\bar{t}\cos(\tfrac{1}{2}\phi\cos\bar{t}) + \zeta^2\sin^2\bar{t})^{\frac{1}{2}}. \tag{21}$$

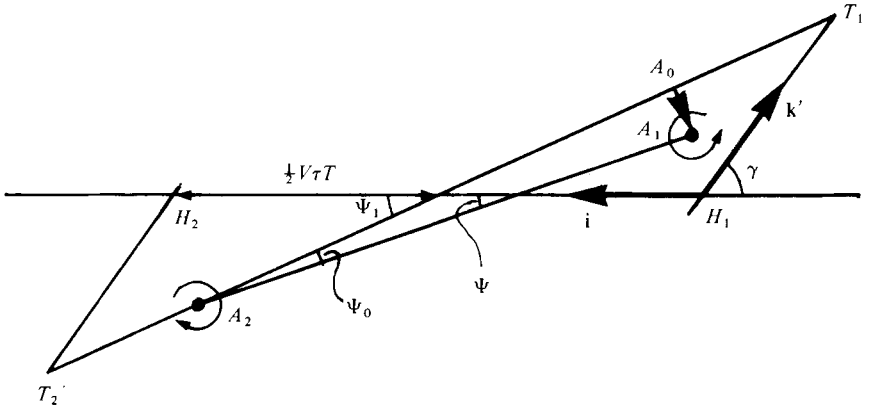

FIGURE 2. Diagram of downstroke geometry, seen from the side (along the $-\mathbf{j}$ direction). Humeral joint moves from H_1 to H_2 and wing tips from T_1 to T_2 approximately along the straight line path shown. The shed vortex ring occupies the plane A_1A_2 at the end of the downstroke; the oldest portion convects from A_0 to A_1. The length A_0A_2 is a fraction R' of the length T_1T_2; Ψ_0 is small, and we can assume that A_0A_2 and A_1A_2 are of equal length.

In hovering flight $\bar{V} = 0$, and (20) may be evaluated to give

$$\mathbf{D}_{\text{pro}} = +0{\cdot}605\,\frac{\rho b^2 S C_{D0}}{\tau T^2}\,\phi J_1(\tfrac{1}{2}\phi)\,\mathbf{k}', \tag{22}$$

where J_1 is a first-order Bessel function; in fast forward flight, as $V \to \infty$, (20) becomes

$$\mathbf{D}_{\text{pro}} \sim -\tfrac{1}{2}\rho S C_{D0}\tau V^2\mathbf{i}, \tag{23}$$

where S is the total wing area

$$2bc_0\int_0^1 \bar{c}(\zeta)\,d\zeta.$$

The momentum $|\mathbf{Q}|$ and inclination Ψ of each elliptical vortex in the wake must be appropriate to sustain and propel the bird for a single wing-stroke (for period T), and so must satisfy (see figure 3)

$$|\mathbf{Q}|(\mathbf{i}\sin\Psi + \mathbf{k}\cos\Psi) = T(Mg\mathbf{k} - \mathbf{D}_{\text{par}} - \mathbf{D}_{\text{pro}}); \tag{24}$$

from (24), $|\mathbf{Q}|$ and Ψ can be found as functions of V and γ.

We now relate Ψ and γ by considering the geometry of the wing-stroke and the shed vortex. Equation (24) then allows solution for all variables as functions of V. The geometry is shown diagrammatically in figure 2; the humeral joint moves from H_1 to H_2, while the wing tips follow an (approximately) elliptical arc from T_1 to T_2. The trailing vorticity is assumed to roll up into a geometrically similar elliptic loop, reduced in dimension by a factor R' (generally $R' < 1$); the ends of the axis of this loop parallel to the forward motion are A_0 and A_2; in fast forward flight this is the major axis, but in slow flight and hovering it can be the minor axis. During the stroke the oldest portion of the vortex loop (the end A_0) is convected downwards through the combined effects of its own vorticity, the bound vorticity on the wings, and the previous wake elements; convection is approximately normal to the free stream, and at the completion of the downstroke the ring lies in the plane A_1A_2. The

convection velocity is a complicated function of many factors and is not constant in space or time; we assume that it can be approximated by the self-induced velocity of the circular ring osculating to the ellipse at A_0; this is an underestimate of the magnitude of the convection and results in underestimates of γ in slow flight.

The geometry shown in figure 2 enables calculation of the vortex-ring proportions; the size R' depends on the wing circulation and is discussed later. Evidently Ψ_1 is given by

$$\tan \Psi_1(\gamma, V) = \frac{b \sin \frac{1}{2}\phi \sin \gamma}{b \sin \frac{1}{2}\phi \cos \gamma + \frac{1}{2} V \tau T}. \tag{25}$$

Since the convection velocity U_{s0} is small compared with V, Ψ_0 will be small in fast forward flight. We can take the length $2b_0$ of the transverse axis of the elliptic vortex ring to be $2bR'$, and the length $2a_0$ of the longitudinal axis to be R' times the length T_1T_2, so that,

$$a_0 = R' \frac{b \sin \frac{1}{2}\phi \cos \gamma + \frac{1}{2} V \tau T}{\cos \Psi_1}. \tag{26}$$

The circulation κ of the vortex ring is defined by the ring momentum and area; the momentum $|\mathbf{Q}|$ is known from the balance of forces on the animal (24), and the area is $\pi a_0 b_0$. Therefore

$$\kappa = |\mathbf{Q}(\gamma, V)|/\rho \pi a_0 b_0. \tag{27}$$

Now, suppose that the vortex has core radius $R_0(a_0 b_0)^{\frac{1}{2}}$, where R_0 is a constant, again depending on the wing circulation. The end A_0 of the vortex ring is assumed to convect with the velocity of a circular ring of radius b_0^2/a_0, which we know [appendix (A 29)] to be given by

$$U_{s0} = \frac{\kappa a_0}{4\pi b_0^2} \left[\log_e \left\{ \frac{8}{R_0} \left(\frac{b_0}{a_0} \right)^{\frac{3}{2}} \right\} - \tfrac{1}{4} \right]. \tag{28}$$

We can solve the system outlined above for $\gamma(V)$ by satisfying the equation

$$\Psi = \Psi_1 - \Psi_0, \tag{29}$$

where $\Psi(\gamma, V)$ is given by (24), $\Psi_1(\gamma, V)$ by (25) and Ψ_0 by

$$\tan \Psi_0 = \tfrac{1}{2} \tau T U_{s0}/a_0. \tag{30}$$

By substitution in the appropriate equation we obtain all variables as functions of V.

It remains to find the size R' and core radius R_0 of the vortex ring. We equate the momentum of the vortex ring to that of the vortex sheet from which it was formed, which can be deduced from the wing circulation distribution $\Gamma(\zeta)$. The technique used to estimate R' is the same as that used in I, § 5 for hovering flight. The area of the portion of the surface $T_1 H_1 H_2 T_2$ (figure 2) mapped out by points at radius ζ on the wings can be written approximately as

$$A(\zeta, \phi) = b^2 \zeta^2 \phi + 2 V b \tau T \zeta J_0(\tfrac{1}{2}\phi). \tag{31}$$

As in I, § 5, only the portion of the sheet for which $\Gamma'(\zeta) < 0$ (say $\zeta > \zeta_0$) can contribute to weight support. Equality of momentum between the ring and this portion of the sheet gives

$$-\int_{\zeta_0}^{1} \Gamma'(\zeta) A(\zeta, \phi) \, d\zeta = \pi R'^2 b \Gamma(\zeta_0) (\tfrac{1}{2} V \tau T + b \sin \tfrac{1}{2}\phi). \tag{32}$$

As in I, §5, the other portion of the sheet has small impulse and energy, and its contributions to the force balance and energy budget are neglected. Writing

$$I_0 = \zeta_0 + \int_{\zeta_0}^{1} \frac{\Gamma(\zeta)}{\Gamma(\zeta_0)}\, d\zeta \tag{33}$$

and

$$I_1 = \zeta_0^2 + 2\int_{\zeta_0}^{1} \zeta \frac{\Gamma(\zeta)}{\Gamma(\zeta_0)}\, d\zeta, \tag{34}$$

we obtain for R' the equation

$$\pi b R'^2 = \frac{b\phi I_1 + 2V\tau T J_0(\frac{1}{2}\phi)\, I_0}{\sin\frac{1}{2}\phi + \frac{1}{2}V\tau T/b}. \tag{35}$$

This agrees exactly with the hovering case when $\phi = \pi\,(V = 0)$; for other ϕ when $V = 0$ the prediction for R' does not differ greatly. Typically R' lies in the range 0·6–0·8 for likely circulation distributions.

In hovering we can reasonably expect that $\Gamma(\zeta) \propto \zeta\bar{c}(\zeta)$ approximately; the above analysis requires $\Gamma(\zeta)$ to be independent of t during the stroke, which is more likely to be satisfied when ϕ is large and circulation can be generated by the 'fling' effect. In forward flight we might expect $\Gamma(\zeta) \propto (1 + \Gamma_1\zeta)\bar{c}(\zeta)$ for some constant Γ_1 depending upon V. Hummel & Möllenstädt (1977) have performed a detailed lifting-surface analysis on the downstroke of a sparrow, for which ample kinematic data exist (Bilo 1971, 1972), and obtained a relationship of this kind. They did not actually quote $\Gamma(\zeta)$, but it may be deduced from other information given. The appropriate values of I_0 and I_1 are respectively 0·79 and 0·64, compared with values of $\frac{1}{4}\pi$ and $\frac{2}{3}$ for elliptic loading ($\Gamma(\zeta) \propto (1-\zeta^2)^{\frac{1}{2}}$).

The non-dimensional core radius R_0 can be obtained only from consideration of the energy of the vortex sheet, a difficult problem which we do not tackle. It appears only as its logarithm, so provided that R_0 is non-zero it cannot affect the problem greatly; a value of 0·171 is known for elliptically loaded rigid wings, and we use this value, together with 0·1 and 0·225, as being likely to span the appropriate range into which R_0 might fall; any variation in R_0 with V is assumed to be small.

4. Power consumption

We have now specified the geometry of the downstroke and of the vortex ring uniquely subject to certain assumptions concerning the mechanism by which the ring is generated, for any velocity V, and are in a position to calculate the rate of working required for sustained steady flight at this velocity. The parasite power is given by

$$P_{\mathrm{par}} = -\mathbf{D}_{\mathrm{par}} \,.\, V\mathbf{i}, \tag{36}$$

so that $P_{\mathrm{par}} \propto V^3$ in fast flight. The profile power is obtained from the total rate of working against profile drag on each wing section. The force $\mathbf{F}_{\mathrm{pro}\pm}$ per unit length on a section of either wing was given by (18), and the velocity $\mathbf{U}_\pm$ of the section by (14). P_{pro} is calculated from the rate of working against profile drag:

$$P_{\mathrm{pro}} = -\frac{\mu b}{T}\int_0^1 d\zeta \int_0^{\tau T} dt\,(\mathbf{F}_{\mathrm{pro}+} \,.\, \mathbf{U}_+ + \mathbf{F}_{\mathrm{pro}-} \,.\, \mathbf{U}). \tag{37}$$

The factor μ is included to take account of the work done during the upstroke to return the wing to the vertical; it is defined as $1+m_s/m_p$, where m_s and m_p are respectively the masses of the muscles powering the upstroke and downstroke; typically it is about 1·1. The correction is small because the wing is flexed during the upstroke to minimize aerodynamic resistance.

With the non-dimensionalization of (16) and (17), we can write

$$P_{\text{pro}} = \frac{\mu\rho b^4 c_0 C_{D0}\phi^3\pi^2}{8\tau^2 T^3}\int_0^1 d\zeta\,\bar{c}(\zeta)\int_0^\pi \bar{U}^3(\zeta,\bar{t})\,d\bar{t}. \tag{38}$$

In hovering, with $\bar{U}=\zeta\sin\bar{t}$,

$$P_{\text{pro}} = 0{\cdot}133\,\mu\rho b^3 S C_{D0}\phi^3/\tau^2 T^3, \tag{39}$$

which agrees with equation (19) of Weis-Fogh (1973). In fast forward flight P_{pro} is proportional to V^3, being V times the expression (23).

The remaining power component is the induced power, the rate of passing mechanical work into the vortex wake to generate momentum which supports and propels the bird. The work done in generating wake kinetic energy can be divided into two components: one is the self-energy of each newly generated ring, the other the interactive or mutual energy between the new ring and each of the existing rings in the wake. The calculation is similar in many respects to that given in detail for the hovering case in I, §4.

We must specify the major and minor semi-axes a_r and b_r of each ring by

$$a_r = \max(a_0, b_0), \quad b_r = \min(a_0, b_0), \tag{40}$$

and then the eccentricity e is given by

$$e^2 = 1 - b_r^2/a_r^2. \tag{41}$$

The calculation of the kinetic energy of an elliptic vortex ring does not appear to have been treated in the literature, and was given particular attention. An algorithm for the calculation of kinetic energy for any smooth closed vortex loop is discussed in the appendix. We quote the formula for the self-energy E_s of the ring defined above from (A 32):

$$E_s = \tfrac{1}{2}\rho\kappa^2 a_r \bar{E}_s, \tag{42}$$

where

$$\bar{E}_s = \frac{2}{\pi}\left\{E(e)\left(\log_e\frac{8}{R_0}-\tfrac{3}{4}\right)-(1-\tfrac{1}{2}e^2)\,K(e)\right\}. \tag{43}$$

K and E are complete elliptic integrals of the first and second kinds. It is assumed in (43) that vorticity is evenly distributed through the vortex core ($\bar{A}=\frac{1}{4}$).

To find the mutual contribution E_m to the kinetic energy we first find the separations $\bar{d}a_0$ and $\bar{h}a_0$ between adjacent members of the chain (figures 3 and 4). In the hovering case the rings were assumed to be circular and coaxial, and it was possible to find $\bar{h}$ exactly for the large family of rings present; $\bar{d}$ was then zero. In the general situation we are discussing here there is no axial symmetry and we cannot predict the interactions of any pair of rings; it is necessary to estimate the velocity of a single element in the chain, and to assume that each ring persists in shape and size at least as long as it can contribute to the induced power. It can be shown (appendix) that an elliptic ring travels with approximately the same velocity as a circular ring of the same impulse and area provided that the eccentricity is not too great ($e^2 \lesssim 0{\cdot}3$), and

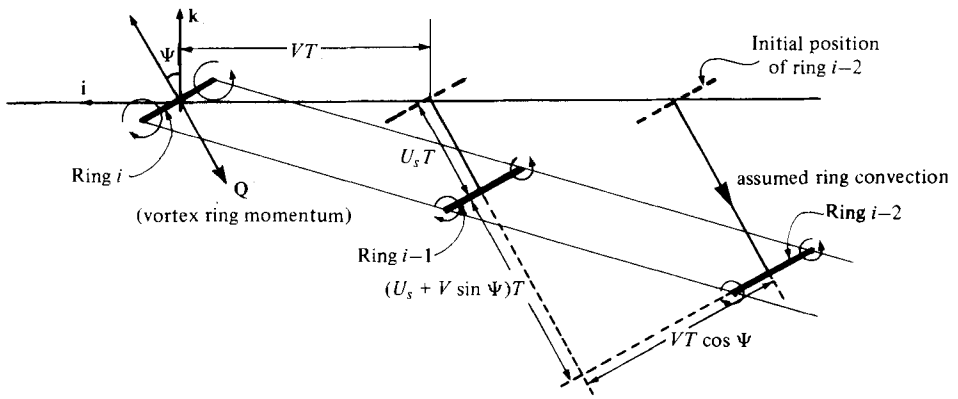

FIGURE 3. Diagrammatic cross-section of the wake of a bird in fast forward flight, relative to still air. Continuous thick lines indicate the positions of vortex rings i, $i-1$ and $i-2$ at the instant when ring i is fully generated; dashed thick lines indicate initial positions of the rings. Note that the downward slope of the wake is caused by ring convection, and that the momentum of each ring (which is normal to the plane of the ring) is not parallel to the wake itself (unless $V = 0$), so that any form of actuator disk or momentum jet description for this flow would not be satisfactory.

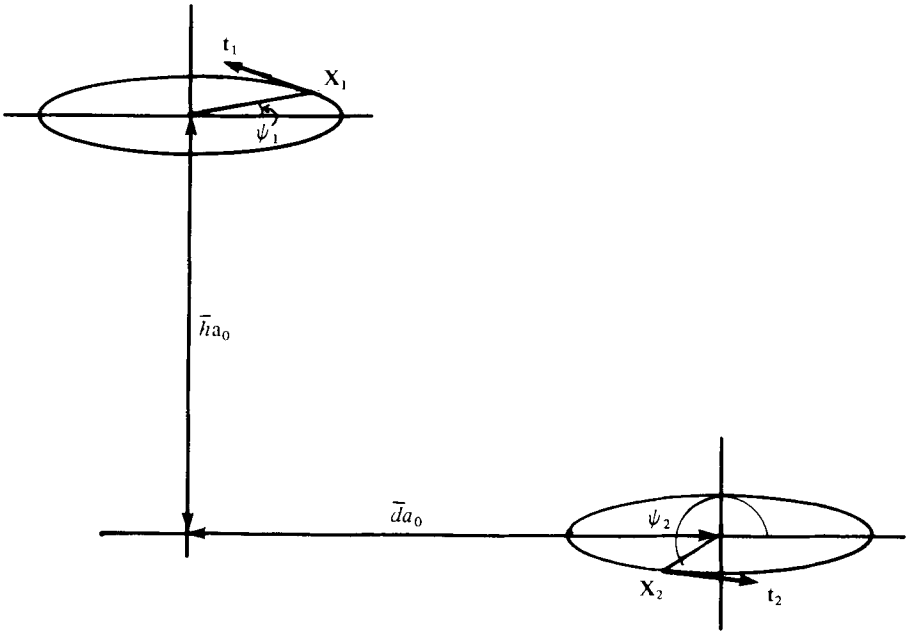

FIGURE 4. Notation for calculation of interactive kinetic energy of two adjacent wake elements in forward flight wake. Lengths $\bar{h}a_0$ and $\bar{d}a_0$ are increased in proportion for other pairs of vortex loops. $\mathbf{X}_1 = (a_0 \cos \psi_1, b_0 \cos \psi_1, 0)$; $\mathbf{X}_2 = (a_0(\bar{d} + \cos \psi_2), b_0 \sin \psi_2, -\bar{h}a_0)$.

further that the rate of deformation will be slow. We estimate the self-convective velocity U_s of a ring from the formula for the equivalent circular ring (A 33), and neglect any motion induced by other rings in the chain. The neglect of the effect of the remainder of the wake is justified by noting that in forward flight of birds individual vortex elements are well spaced, so that the dominant convection velocity on

any ring is its own self-convection. This is

$$U_s = \frac{\kappa}{4\pi(a_0 b_0)^{\frac{1}{2}}}\left(\log_e \frac{8}{R_0} - \tfrac{1}{4}\right); \tag{44}$$

thus the separations between rings are

$$\bar{d} = (VT/a_0)\cos\Psi \tag{45}$$

and

$$\bar{h} = (V\sin\Psi + U_s)\,T/a_0. \tag{46}$$

These results can be only an estimate of the true spacing for a number of reasons. They assume that all rings in the wake persist, which is not fully acceptable even for an isolated elliptic ring unless the eccentricity is small; moreover in this application each ring is in a very complicated velocity field. Accurate results for the induced power in hovering are available in I, §7, and are close to the predictions of this calculation; as the forward velocity increases the mutual induced power falls off very rapidly, and is negligible when the eccentricity is large enough to make ring distortion a real problem. The difficulties of calculating the ring shape and spacing in the far field exactly at all times are insuperable, and their neglect is justified by the availability of an exact solution when V is zero, and the insignificance of the mutual contribution to induced power when V becomes large.

To calculate the interactive energy of two rings (1 and 2) we use the formula

$$E_m^{1,2} = \frac{\rho\kappa^2}{4\pi}\oint\oint \frac{\mathbf{t}(s_1)\,.\,\mathbf{t}(s_2)}{|\mathbf{X}_1 - \mathbf{X}_2|}\,ds_1\,ds_2, \tag{47}$$

as in I, §4, equation (44). The notation is shown in figure 4. In particular

$$\mathbf{X}_1 = (a_0\cos\psi_1, b_0\sin\psi_1, 0) \tag{48}$$

and

$$\mathbf{X}_2 = (a_0(\bar{d} + \cos\psi_2), b_0\sin\psi_2, -\bar{h}a_0), \tag{49}$$

so that

$$E_m^{1,2} = \frac{\rho\kappa^2}{4\pi}\int\int_0^{2\pi} \frac{(a_0^2\sin\psi_1\sin\psi_2 + b_0^2\cos\psi_1\cos\psi_2)\,d\psi_1 d\psi_2}{[a_0^2(\cos\psi_1 - \cos\psi_2 - \bar{d})^2 + b_0^2(\sin\psi_1 - \sin\psi_2) + a_0^2\bar{h}^2]^{\frac{1}{2}}}. \tag{50}$$

The total mutual energy is the sum of the contributions from interaction with each other member of the chain:

$$E_m = \tfrac{1}{2}\rho\kappa^2 a_r \bar{E}_m, \tag{51}$$

where

$$\bar{E}_m = \frac{a_0}{a_r}\sum_{n=1}^{\infty} f_m^n\left(\frac{b_0}{a_0}, \bar{d}, \bar{h}\right), \tag{52}$$

and f_m^n can be derived from $E_m^{1,2}$ as

$$f_m^n(\bar{b}, \bar{d}, \bar{h}) = \frac{1}{2\pi}\int\int_0^{2\pi} \frac{(\sin\psi_1\sin\psi_2 + \bar{b}^2\cos\psi_1\cos\psi_2)\,d\psi_1 d\psi_2}{[(\cos\psi_1 - \cos\psi_2 - n\bar{d})^2 + \bar{b}^2(\sin\psi_1 - \sin\psi_2)^2 + n^2\bar{h}^2]^{\frac{1}{2}}}. \tag{53}$$

f_m^n is small for large n compared with $\bar{E}_s$ and f_m^1, and rings in the far field make no significant contribution to the mutual energy. In fast forward flight the sum in (52) converges within about five terms. In slow flight more terms are needed.

The induced power P_i is calculated as a function of V from the total energy increment [sum of (42) and (51)] divided by the stroke period; thus

$$P_i = \tfrac{1}{2}\rho\kappa^2 a_r(\bar{E}_s + \bar{E}_m)/T. \tag{54}$$

The total flight power $P(V)$ is the sum of the parasite, profile and induced components [(36), (38) and (54)]:

$$P(V) = P_{\text{par}} + P_{\text{pro}} + P_i. \tag{55}$$

This equation enables us to calculate $P(V)$ as a function of V for any realistic combination of kinematic parameters ϕ, τ and T.

In hovering the parasite power is negligible and the profile power small; both increase approximately as V^3, and are dominant in fast forward flight. The induced power is large in hovering, and falls rapidly as V increases, finally decaying approximately as V^{-1}. The $P(V)$ curve is thus U-shaped, with a definite speed V_0 at which power consumption is a minimum. The behaviour of this curve as kinematic and morphologic parameters vary is one of the main factors determining a bird's flight style, since it must always be concerned to reduce power consumption at its chosen flight speed.

5. Lift coefficient

The main advantage of the vortex theory is the absence of any assumptions regarding the magnitudes of lift and induced drag coefficients, which have in varying ways been present in most former avian power calculations. It would be hard, if not (in our present state of knowledge) impossible, to derive these coefficients accurately for a bird's reciprocating wing under all possible conditions. They of course vary both across the wing-span and during the stroke in an unpredictable way; only if the flow could be assumed to be sufficiently steady would a lifting-line or lifting-surface theory give their values instantaneously. An analysis of this kind on the sparrow in fast forward flight (9 m/s) has been attempted by Hummel & Möllenstädt (1977) at the instant when the wings are horizontal. Their results show that (passing outwards along the wing) C_L rises slightly over the inner portion to a maximum of 0·7 at the midpoint of the wing, and then falls rapidly to zero at the wing tip; the mean C_L is about 0·3. They suggest that at their Reynolds number of 10^4 the value $C_L = 0{\cdot}7$ is near to the maximum that the wing can sustain, although perhaps this is overcautious, and can be meaningful only when the variation of C_L with time is known. These figures imply that a quasi-steady analysis may be satisfactory at high forward velocities, but not at low velocities or in hovering, when the lift coefficients required would rise well above a reasonable maximum of 1·5 or 2 consistent with the steady-state theory. Observations of the pied flycatcher *Ficedula hypoleuca* and associated calculations by Norberg (1975) give a disturbingly high mean C_L of 5·3 in hovering; although we recalculate the figure as 4·1 this is still much larger than any value consistent with steady-state wing theory. Norberg (1976*a*, *b*) estimates C_L to be between 3·1 and 6·4 in hovering and about 1·5 in forward flight at 2·35 m/s for the long-eared bat *Plecotus auritus* (body mass 9×10^{-3} kg), again suggesting that unsteady effects are responsible for lift.

By avoiding force coefficients (except for the simpler wing profile drag) we are less bound by the steady-state assumptions and can give a more reliable estimate of flight power. We are no nearer to investigating the means by which such high levels of circulation can be attained on the wing. To this outstanding problem in any study of animal flight, the few existing clues are as follows. There are a number of modifications to the bird's wing which can probably assist generation of high levels of lift in

flight (leading-edge slots, primary-feather twisting and separation, chordwise deformation under aerodynamic load, elastic bending of feathers) which have been widely studied (Oehme & Kitzler 1974, 1975*a*; Nachtigall & Kempf 1971; Pennycuick & Lock 1976). The main enigma is the function of primary-feather separation; this occurs in many species under particularly exacting flight conditions, and the smallest passerine birds use it at all times. It certainly has a valuable aerodynamic effect, but the exact mechanism has not been discovered; presumably lift enhancement, boundary-layer control and induced-drag reduction are all relevant.

Some recent research into the use of 'sails' at the wing tips of aircraft (Spillman 1979) has shown that the induced drag can be significantly reduced, without an increase in the other drag components, and therefore with some saving in flight power. Geometrically these sails are similar to the separated primary feathers found in many small birds and in larger birds which use static soaring (e.g. birds of prey) or with disproportionately small wings (e.g. gallinaceous birds); although the research applies to the rigid wing of aircraft it is likely that the same (or at least a related) mechanism operates on a bird's wing in flapping flight, and there can be little doubt that this is the reason for feather separation in soaring birds.

The sails have the effect of causing the wing-tip vortices to spiral outwards so that the final separation is greater than if the wing were unmodified. If the same effect occurs in avian flapping flight the vortex-ring size R' would be increased. We know that a larger R' implies lower induced power, since the vortex ring must have the same momentum (assuming that separation does not materially increase profile drag); the momentum is proportional to $\kappa R'^2$, from (27), so that the circulation κ can be reduced. From (42) we see that the self-energy of each vortex ring is proportional to $\kappa^2 R'$, so that the self-energy contribution to the induced power is approximately proportional to R'^{-3}; this increase in R' gives a small increase in mutual energy, but the overall effect is for the induced power to be reduced.

In view of this possible effect of separation it may be that we are using unrealistically low values of R' in some cases. Until more information on the details of the mechanism for a bird's wing is available we cannot do better than use the values calculated in § 3; we should be able to take account of separation either by modifying the form of $\Gamma(\zeta)$, or alternatively by introducing a suitable 'aerodynamic wing span', greater than $2b$, across which circulation might be elliptic; this could synthesize the effect of separation by replacing the modified wing with the equivalent, larger, simple wing.

A valuable discussion of the aerodynamic functions of a bird's wing, including consideration of such properties as through-wing suction, has been given by Vinogradov (1951); this paper contains a good deal of interesting argument not available elsewhere.

Another possible way for a bird to obtain high lift and high wing circulation is by the Weis-Fogh clap-and-fling mechanism (Lighthill 1973), which may be important to pigeons and doves for instance, or other as yet undiscovered effects of the same kind. While we cannot specify the way in which high values of circulation are achieved, we can recall that since the birds can fly, somehow they are practicable. The vortex theory will not be greatly affected by unsteady effects provided that we assume that they are consistent with the rapid roll-up of the vortex sheet into an elliptic vortex loop.

To estimate the lift coefficients required we give below a simple theory for their calculation, similar to the profile-power calculation in §4.

The vertical component $L_\pm$ of the sectional lift force on the $\pm$ wing is given by

$$L_\pm = \pm \tfrac{1}{2}\rho c_0 \bar{c}(\zeta) C_L U \mathbf{U}_\pm \wedge \mathbf{t}_\pm . \mathbf{k}, \tag{56}$$

assuming a *mean* lift coefficient C_L. The total lift must balance the weight of the bird, so that allowing for the vertical components of parasite and profile drags, we have

$$\frac{b}{T}\int_0^{\tau T} dt \int_0^1 d\zeta\,(L_+ + L_-) = Mg - (\mathbf{D}_{\mathrm{par}} + \mathbf{D}_{\mathrm{pro}}) . \mathbf{k}. \tag{57}$$

Any lift derived from induced drag is neglected on the right-hand side of (57). From these equations we may determine C_L. In hovering, profile drag is negligible, and then

$$C_L = 6{\cdot}62\, Mg\tau T^2/\rho b^2 S\phi^2 \cos\gamma \tag{58}$$

which is the maximum C_L needed in steady flight; higher values are required in take-off. We relate the hovering C_L to the feathering parameter f (defined in I, equation (16) as $MgT^2/2\pi^3\rho b^4$) and the aspect ratio A_r (wing span squared divided by total wing area, i.e. $4b^2/S$) by the formula

$$C_L = 102{\cdot}6\,\tau f A_r/\phi^2 \cos\gamma, \tag{59}$$

so that birds with low f and low A_r are more likely to overcome the aerodynamic constraints on lift generation in hovering. It was shown in I, §7 that low f also implies low hovering induced power; evidently a low feathering parameter (i.e. a high wing span and/or a low stroke period) is of great importance if the bird is to be able to hover or fly slowly.

At higher speeds C_L decays approximately as V^{-2}; it is small, and does not represent a significant constraint. We cannot deduce optimum morphologic conditions for fast flight on the basis of lift generation, but the magnitude of the hovering lift coefficient [(58) or (59)] indicates the importance of the constraint in hovering, slow flight and take-off. From it we can deduce whether hovering is at all possible, or whether it is possible only with unsteady lift generation.

With $\phi = 100°$ and $\gamma = 30°$ (the configuration observed by Norberg), we evaluate (58) for the flycatcher to obtain $C_L = 4{\cdot}1$; with the same ϕ and γ we can find further that for the wren $C_L = 20{\cdot}6$, for the pigeon $C_L = 10{\cdot}3$, for the mallard $C_L = 11{\cdot}9$ and for the pheasant $C_L = 11{\cdot}4$. Of these birds, only the flycatcher is known to hover with such a small value of ϕ. The pigeon hovers occasionally with $\phi \approx 180°$, and then $C_L = 3{\cdot}2$; it probably takes advantage of the clap-and-fling mechanism. Some similar form of lift enhancement is probably being used by the flycatcher.

6. Applications

We consider in this section the behaviour of the model and the influence of various of the parameters included in it. A detailed discussion of the biological findings will be found in Rayner (1979*b*, §4). That section includes discussion of the influence of morphologic and kinematic parameters on flight style and power consumption for a number of species.

To illustrate the discussion in the next sections we perform calculations on data

Body mass, M (kg)	0·012
Wing semi-span, b (m)	0·115
Wing area, S (m^2)	0·0090
Pectoralis major relative mass, m_p/M	0·16*
Muscle ratio, μ	1·10*
Stroke Period, T/s	0·07
Feathering parameter, f	0·044
Aspect ratio, A_r	5·9
Disc loading, N_d/N m^{-2}	2·8

TABLE 1. Morphologic data for pied flycatcher *Ficedula hypoleuca*, from Norberg (1975) (* from Greenewalt 1962).

for the pied flycatcher. The appropriate morphologic data are given in table 1. This bird is selected because it is the only species for which a complete set of observations of morphologic and kinematic parameters is available (Norberg 1975), albeit only for hovering. Very similar conclusions as to the influence of stroke parameters, or of drag representation, on flight power are made for other species and there is no danger that selecting a single bird in this way will distort our results.

The calculations were carried out using the IBM-370 at Cambridge; because of the complexity of the model they were costly in computing time and the number of applications had to be restricted. Mks units are used throughout.

All of the calculations rely heavily on data obtained (mainly in the field) from real birds. For many reasons we must expect the errors in the measurements, and further the errors we introduce in assuming that a handful of specific measurements may apply to a species as a whole, to be sizeable. As data relevant to avian flight are scanty we cannot attempt to make any estimate of the magnitude of the error. We may be reassured, however, by noting that many of our conclusions refer to deductions relative to two parameters or to two species, so that even if the magnitude of the power consumption is unreliable we may make valuable conclusions. Moreover, as in many biological problems, maxima and minima are shallow, so that (for instance) a moderate change in flight velocity will result in a small change in power. We may therefore expect the various deductions we make to be insensitive to inaccuracies in data.

The main feature of the model which we discuss here is the representation of the parasite drag, which was explained fully in §3; the effect of varying this is given in §8. We must also consider the influence of the magnitude of the profile-drag coefficient C_{D0}, the size R' and core radius R_0 of each vortex ring, and of the ring convection velocity estimated by (28). We also give a very brief discussion of the influence of kinematic and morphologic parameters.

7. The power curve

It has already been stated that as the flight velocity increases, the induced power drops, and parasite and profile powers rise, the net result being a U-shaped curve of total aerodynamic power against velocity. A sample power curve for the flycatcher is shown in figure 5. It is clear that this curve defines two characteristic velocities: V_0, at which the total power $P(V)$ is minimized [$(V_0) = P_0$], and V_1, at which the cost

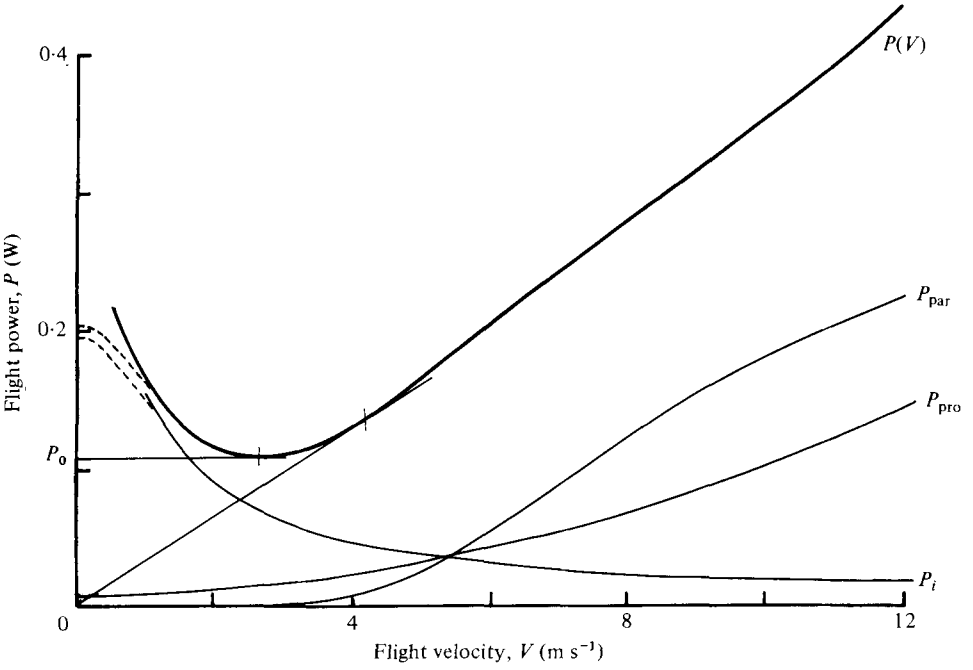

FIGURE 5. Power curves for pied flycatcher *Ficedula hypoleuca* (M = 0·012 kg); with $\phi = 120°$, $\tau = \frac{2}{7}$, standard drag representation (see §8), $R_0 = 0{\cdot}171$; $I_0 = 0{\cdot}896$, $I_1 = 0{\cdot}808$. Dashed portions of the curves at low velocity are interpolations from the exact hovering induced power calculated in I. Note the high parasitic power and associated low minimum cost speed, but almost constant cost of transport at high speeds.

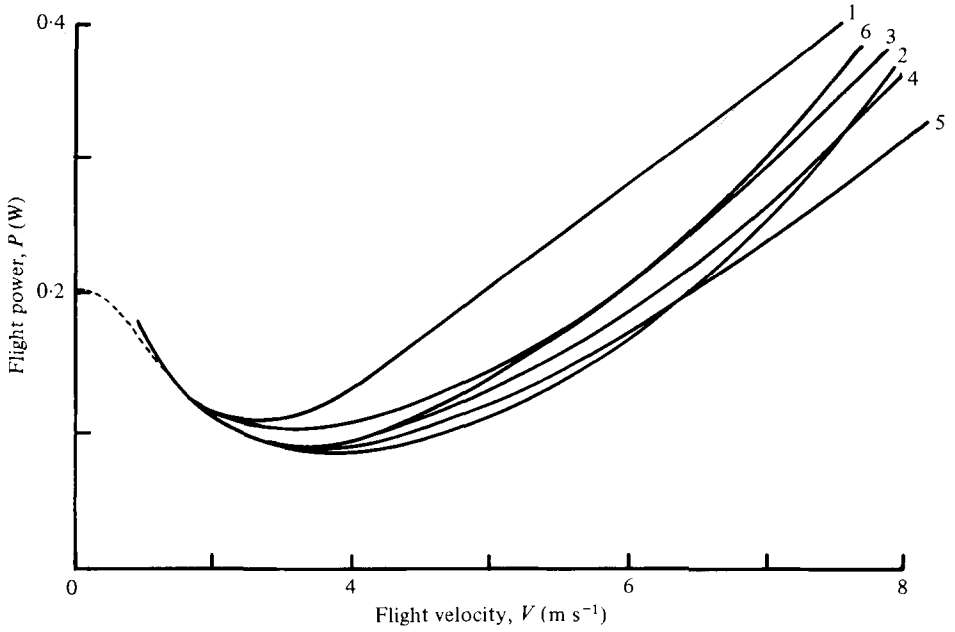

FIGURE 6. Comparison of effect on power consumption of different drag representations, for flycatcher. Apart from drag representation the parameters are as in figure 5. Curve 1, standard body drag, $A_b = 0{\cdot}045\, M^{\frac{2}{3}}$, $\beta = 80° - \gamma$; 2, standard body drag, body untilted (i.e. $\beta = 0$); 3, standard body drag, $A_b = 0{\cdot}01\, M^{\frac{2}{3}}$, $\beta = 80° - \gamma$; 5, standard body drag, $A_b = 0{\cdot}045\, M^{\frac{2}{3}}$, $\beta = 45° - \gamma$; 5, Csicsáky drag, $\beta = 55° - \gamma$; 6, double Csicsáky drag, $\beta = 55° - \gamma$.

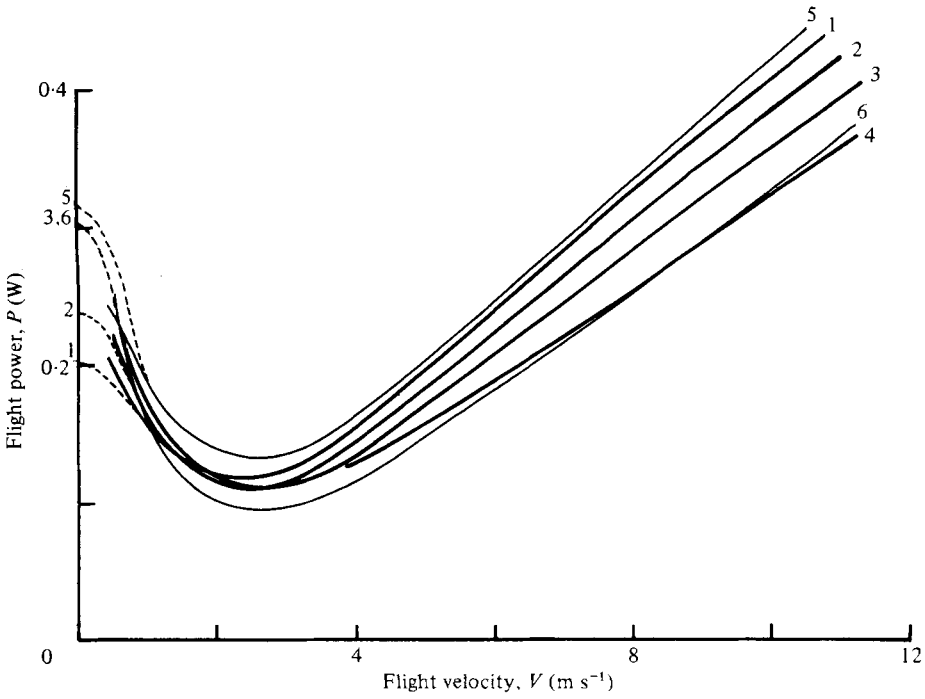

FIGURE 7. Effect on power consumption of varying kinematic parameters, for flycatcher; other parameters and features as in figure 5. Curves: 1, $\phi = 180°$, $\tau = \frac{3}{7}$; 2, $\phi = 150°$, $\tau = \frac{3}{7}$; 3, $\phi = 120°$, $\tau = \frac{3}{7}$; 4, $\phi = 90°$, $\tau = \frac{3}{7}$ (not shown for small V); 5, $\phi = 120°$, $\tau = \frac{2}{7}$; 6, $\phi = 120°$, $\tau = \frac{4}{7}$.

of transport $C(V)$ is minimized [$C(V_1) = C_1$]; V_1 is greater than V_0. The minimum is very shallow and there is little increase in power or cost with a moderate change in velocity. The hovering induced power is calculated from the results of I [equation (80)] since this calculation is more accurate at low speeds than the limiting form of the forward-flight model described in this chapter; where appropriate the low-speed values of the power are interpolated by eye, and are indicated in figure 5 by dashed lines.

The cost of transport referred to above, defined by

$$C(V) = P(V)/MgV, \tag{60}$$

measures the aerodynamic work done in transporting a unit weight through unit distance; it is therefore a non-dimensional quantity. The bird will choose to fly at the minimum cost speed V_1 if it must cover a great distance, since at this speed the total energy required is least although the power required is above the minimum. In other conditions, particularly for short flights, the bird is more likely to select the minimum power speed V_0. The curve of power consumption against velocity for a bird in flapping flight has much in common with the glide polar for a gliding bird or aircraft; there are the same characteristic speeds, and the possibility of stall at some low forward velocity around the minimum power speed if the wings cannot produce sufficient lift to keep the bird aloft. The extra relative air speed due to flapping pushes the stall velocity lower than in gliding, and some birds are capable of hovering; some

species can hover for short periods only, and we deduce that in these cases metabolic power is the limiting factor.

By altering the few morphologic parameters under its control a gliding bird can obtain access to the envelope of a family of glide polars, various of which might be more favourable at different glide speeds or descent angles; Lighthill (1974) has shown that a gliding bird should spread its wings at lower velocities. By varying the kinematic parameters with only minor changes to the morphologic parameters a flapping bird can reach a similar envelope of a family of power curves. It will choose the most advantageous configuration within the limits of its aerodynamic and structural capabilities. (We have seen in §5 how lift generation is an important consideration.) We consider the benefit to be gained from varying the kinematic and morphologic parameters in §10 and in greater detail in Rayner (1979*b*, §4).

While the two speeds V_0 and V_1 characterize the power curves, they are not necessarily the speeds which minimize the cost to the fuel reserves per unit time or per unit distance. V_1 will vary if there is a head or tail wind, since this calculation is concerned with flight relative to still air, and the cost of transport is useful only when considered as energy per unit ground distance; in addition V_1 will increase if we include a fixed basal metabolism to account for energy consumed by internal body functions independent of flight.

The stroke-plane angle γ predicted by the model is generally too small in hovering and slow flight, especially for birds with low f. Predictions for the flycatcher in hovering are too small by up to a factor of approximately 2·5; as V increases γ rises and reaches realistic values at around the minimum cost speed. The discrepancy is caused by the inaccuracy of the formula (28) for the convective velocity U_{s0} of the vortex ring; this formula neglects the induced velocity due to vorticity elsewhere in the flow field, and therefore underestimates U_{s0}. When f is small older wake elements are close to the bird in forward flight, so the underestimate is greater. In fast forward flight the predicted γ is generally in the range 60–75°, which is wholly realistic. The variation of $\gamma(V)$ with such factors as the drag representation considered in §§3 and 8 is slight.

Although $\gamma(V)$ is inaccurate at low speeds, the inaccuracy does not materially affect the total power consumption calculated. By modifying the form of U_{s0} it can be shown that the power consumption is very insensitive to the values of γ, i.e. that the zeros of (29) are very shallow and are not greatly affected by substantial changes in $\gamma(V)$, consistent with the representation of convection. In view of the extreme difficulty in expressing U_{s0} exactly at low speeds and the insensitivity of total power to its value we neglect this problem.

8. Drag representation

We have seen in §3 that there are a number of different ways of representing body parasitic drag. The effect of these on the power is shown in figure 6 for the flycatcher with $\phi = 120°$. Similar effects are found for other species.

The 'standard' body drag given by (5)–(7) with $\beta = 80° - \gamma$ gives the greatest power consumption, substantially greater than other alternatives at medium speeds (curve 1). It has the interesting property that for a broad range of speeds $P(V)$ is proportional to V, so that the cost of transport is constant and minimum. This is true to some extent for most species; while it may be a useful adaptation allowing

minimum cost to be reached at quite high speed, it is more likely to be coincidental since the presence of a tail wind would dramatically reduce the benefit. It is possible that the value ascribed to A_b in (7) is remarkably high; however, reducing this by a factor of 4 does not greatly alter the total power (curve 3), so the high A_b need not be of great disadvantage to the bird.

Relaxing the relation between β and γ to $\beta = 45° - \gamma$ allows a much reduced P_0 and C_1, with a valuable increase in V_1 (curve 4); perhaps this is a more realistic configuration for many birds than curve 1. If the body were to remain untilted at all speeds ($\beta = 0$; curve 2) P_0 and C_1 would be low; the penalty of a low V_1 is not significant when the cost is so small, but it is unlikely that many birds can take advantage of this strategy.

Finally, we see that the representation of Csicsáky, given in (8) and (9) with $\beta = 55° - \gamma$ (curve 5), has, as expected, very much lower power consumption at high speeds than any of the other forms. Doubling the magnitude of each of the Csicsáky drag components gives a more realistic estimate (curve 6) which is comparable with the other drag representations.

The profile drag coefficient C_{D0} was tentatively assigned the value 0·02 in §3. Varying this has a largely predictable, and generally insignificant, effect. With a large increase in C_{D0} to 0·04, there is a small rise in P_0 and C_1, a slight fall in V_1 and a rise in V_2; the minima of P and C both become more shallow.

It is difficult to select the optimum drag representation, especially as this probably varies widely between species. We use the 'standard' form of (5)–(7), with $\beta = 80° - \gamma$ and with $C_{D0} = 0{\cdot}02$. This may lead to a slight overestimate of power at all velocities, but it is perhaps better to be pessimistic. The relative effects of varying the kinematic parameters are not affected by the drag representation used.

9. Tolerance to features of the model

In the formulation of the model there was a number of features of a rather specific nature which had to be left undecided, since the use of more accurate representations would have required an unrealistic amount of calculation. As was stated in §3, the ring convection velocity U_{s0} could be varied with only a small ($\approx 1\%$) change in the total power; we can therefore use (28) with reasonable confidence, despite the associated underestimate of γ at low speeds.

We must also consider varying the wing-circulation constants I_0 and I_1, and thus the vortex-ring size (but not shape) and the vortex-ring core radius R_0; I_0 and I_1 are related to the circulation $\Gamma(\zeta)$ by (33) and (34). If the loading is elliptic, i.e. if

$$\Gamma(\zeta) \propto (1-\zeta^2)^{\frac{1}{2}},$$

then $I_0 = \frac{1}{4}\pi$ and $I_1 = \frac{2}{3}$; it is proportional to span times wing chord $\Gamma(\zeta) \propto \zeta\bar{c}(\zeta)$, $I_0 = 0{\cdot}896$ and $I_1 = 0{\cdot}808$. The circulation distribution found by Hummel & Möllenstädt (1977) leads to the values 0·79 and 0·64, so that we can reasonably expect I_0 to lie in the range 0·70–0·90 and I_1 to lie in the range 0·55–0·85. All other variables being unchanged, we find that the range of ring sizes specified by this spread of circulation constants leads to insignificant changes in total power consumption in forward flight, and a range of variation in induced power in hovering of at most $\pm 10\%$ [see I,

equation (80)]. There is no loss of accuracy in forward flight if the values associated with $\Gamma(\zeta) \propto \zeta\bar{c}(\zeta)$ are selected, i.e. $I_0 = 0{\cdot}896$ and $I_1 = 0{\cdot}808$.

There was also some doubt about the value which should be assigned to the ring core radius R_0. It is possible that R_0 should depend on the forward velocity and kinematic parameters. The dependence of U_{s0} and the kinetic energy on R_0 is logarithmic, so any effects of varying R_0 within the range for which the ring may still be considered to have a finite small core, i.e. for which $R_0^2 \ll 1$ and $R_0 \neq 0$, will be small. We choose a mean value of 0·171, associated with elliptic loading of a rigid wing, and consider variations within the range 0·1–0·225. The effect of this range on P_0 and C_1 is small, being $\pm 10\%$ at most. This range spans the values R_0 is likely to take: if anything it will lie towards the upper end ($R_0 \approx 0{\cdot}2$), since the circulation distribution is likely to be less efficient than the optimum elliptic form.

It is difficult to select a representative combination of parameters and definitions which is equally realistic in all possible conditions. On the basis of the arguments given above we choose the 'standard' form of drag given by (5)–(7), with $\beta = 80° - \gamma$, $R_0 = 0{\cdot}171$, $I_0 = 0{\cdot}896$ and $I_1 = 0{\cdot}808$, and with the convection velocity U_{s0} given by (28). We use this combination in the investigation of flight style described in §10 and in Rayner (1979*b*, §§4 and 5).

10. Kinematic parameters and flight style

We are now in a position to make the most important deductions from the model: those concerning the flight style dictated by a choice of kinematic parameters. The morphologic parameters M, b, c_0 and S are assumed to remain fixed at all speeds; this is equivalent to stating that the wings do not flex in any way at higher speeds, but have the same planform throughout the downstroke at all velocities. We assume that the stroke period T is likely to be constant for any individual; the stroke-plane angle γ is determined by the momentum balance in the model, and in any case does not affect power consumption. The only parameters which we are able to vary are therefore the stroke amplitude ϕ and downstroke ratio τ.

The requirements predicted by the model on ϕ and τ are clear (figure 7). In hovering, induced power dominates and I, equation (80), shows that τ is largely irrelevant, but that a large value of ϕ is beneficial; a large ϕ also lowers the lift coefficient required, so it is clearly important. In fast forward flight profile and parasitic powers domiante; ϕ can be small and τ large, as far as is consistent with lift generation. Many large birds are able to adjust to the limit $\phi \to 0$ and $\tau \to 1$, which represents gliding, 'power' consumption is then measured by the rate of height loss. To glide efficiently a bird requires a high aspect ratio and low disk loading, since this reduces power consumption in steady level flight.

We can see from figure 7 that somewhere around the minimum power speed V_0 the optimum values of ϕ and τ change rapidly; this corresponds to the transition from slow to fast forward flight, and agrees well with observations of the swift (Oehme 1968) and the gull (Tucker 1972), in which the flight style was found to change markedly between the two modes of flight. Although figure 7 illustrates the effect of varying the kinematic parameters for the flycatcher only, the conclusions are valid for all species since similar graphs are observed for other birds. There is always the same preference for a high ϕ in slow flight and a low ϕ in fast flight, with a high τ

throughout if power reduction is to be the main criterion for the choice of flight style. In slow flight lift generation can be critical (§5), and this strategy will also ensure that the lowest lift coefficients are needed, and hence that the aerodynamic demands on the wing are less exacting.

It is also of great interest to consider the interrelation between a bird's life style (ecology and habitat, for example), its power consumption and its morphology. As we should expect, these factors have a considerable influence on one another, for the shape of the power curve reflects the morphological characteristics, and in its turn dictates the optimum flight style. We discuss this topic at greater length in Rayner (1979*b*).

11. Conclusions

(i) A theory is given by which the wake of a bird in steady level forward flight is modelled as a chain of elliptic vortex rings. This allows calculation of power consumption and of mean lift coefficients.

(ii) Existing theories place too much reliance upon force calculation from lift and drag coefficients. Lift coefficients obtained from measurements of birds and bats in slow flight are too high to be consistent with steady-state aerodynamics. No unsteady theory is available to describe avian flight, but the analysis in terms of wake vorticity circumvents the use of lift and induced drag coefficients.

(iii) For the purposes of this theory a bird may be characterized by four morphologic parameters, viz. the mass, wing-span, wing chord and muscle ratio, together with four kinematic parameters, viz. the stroke period, downstroke ratio, stroke amplitude and stroke-plane angle.

(iv) The wake consists of a chain of elliptic vortex rings, each planar and of small core radius. Each downstroke generates a single ring; the dimensions of the ring are determined by the kinematics of the downstroke and by the wing circulation distribution. The forces on the bird (weight plus sum of parasitic and profile drags) must be balanced by the mean rate of increase of wake momentum. The bird's equation of motion allows us to determine the geometry of the downstroke and the circulation of the vortex ring.

(v) The upstroke is aerodynamically very lightly loaded and does little or no useful work. It therefore leaves no trailing vorticity. We can assume that the vortex elements shed by successive downstrokes are discrete from each other.

(vi) Various representations of parasite drag, depending upon the body configuration and the degree of flexibility around the humeral joint, do not have a significant effect on power consumption.

(vii) The power consumed in forward flight is calculated as the rate of working against parasite and profile drags plus the rate of supply of kinetic energy to the wake; the three components are the parasite, profile and induced powers. The induced power dominates in slow flight, the parasite and profile powers in fast flight; the power against velocity curve is U-shaped.

(viii) The theory given here can be extended to cover hovering, but the results are then less accurate because the aerodynamic interaction between wake elements is not considered. The previous paper discussed the hovering case exactly, and the results for the induced power in hovering can be quoted from there. In forward flight

the elements become separated and interaction is minimal; the induced power is small and moreover is dominated by the contribution from the newest ring; older rings further down the chain need not be considered. Equally, self-deformation of each wake element occurs significantly only in fast forward flight (when the eccentricity is large), and its neglect can be justified by the small contribution the induced power then makes to the total power.

(ix) The pattern of kinematic parameters that a bird may choose is described as *flight style*; this can vary with the flight mode. The range of kinematic parameters available is limited by the strength of the bones and muscles concerned, in addition to the velocity-dependent constraint of lift and thrust generation. The bird must select the parameters within these limits which minimize the rate of working; in slow flight this corresponds to a large stroke amplitude ϕ, and in fast flight to as small a value of ϕ as possible, with as large a value of the downstroke ratio τ as can be achieved.

Appendix. Induced velocity and kinetic energy of vortex loops

Many problems in unsteady aerodynamics require knowledge of the behaviour of various forms of vortex systems. In particular, we often require the distribution of induced velocities due to a vortex loop, and the kinetic energy of that system. The kinetic energy is the work done in setting up the vorticity in otherwise undisturbed fluid. Unless the vortex loop is circular it will not persist undeformed; in this case the induced velocity and kinetic energy must be considered as instantaneous values. The expressions for the induced velocity and kinetic energy of a small-cored circular vortex are well known (e.g. Lamb 1932, art. 163). Widnall & Sullivan (1973) have considered the stability of the circular ring to radial sinusoidal perturbations; in the course of this work a method is given for the calculation of the self-induced velocity of a curved vortex line (see also Widnall, Bliss & Zalay 1971); we reformulate this calculation below. Saffman (1970) discusses the influence of viscosity on a circular vortex ring, giving a simple derivation of the energy of such a system. All of these calculations assume that the core radius is small and finite; Fraenkel (1970, 1972) has proved that the familiar expressions for velocity and energy are valid asymptotically as the core shrinks, while Norbury (1973) has shown the existence of a family of rings with arbitrary core, whose other limit is Hill's spherical vortex.

We are concerned here with the calculation of the induced velocity at a point on the vortex and the kinetic energy of a smooth closed vortex loop of circular cross-section everywhere small compared with the local radius of curvature. We consider the induced velocity first.

Vorticity is distributed over a volume V with strength $\boldsymbol{\omega}(\mathbf{x})$, $\boldsymbol{\omega}$ being the flux of circulation per unit area. The induced velocity $\mathbf{u}_i$ at $\mathbf{x}'$ is given by the Biot–Savart law:

$$\mathbf{u}_i(\mathbf{x}') = -\frac{1}{4\pi}\iiint_V \frac{(\mathbf{x}'-\mathbf{x})\wedge\boldsymbol{\omega}(\mathbf{x})}{|\mathbf{x}'-\mathbf{x}|^3}\,d^3x. \tag{A 1}$$

Let the centre-line of the vortex loop be parameterized by the arc length s ($0 \leqslant s \leqslant \Sigma$); the local tangent vector is $\mathbf{t}(s)$ and other unit vectors are defined by $\mathbf{n}(s)$, parallel to $d\mathbf{t}/ds$, and $\mathbf{b}(s) = \mathbf{t}(s)\wedge\mathbf{n}(s)$ (see figure 8). The local radius of curvature is $R(s)$ while

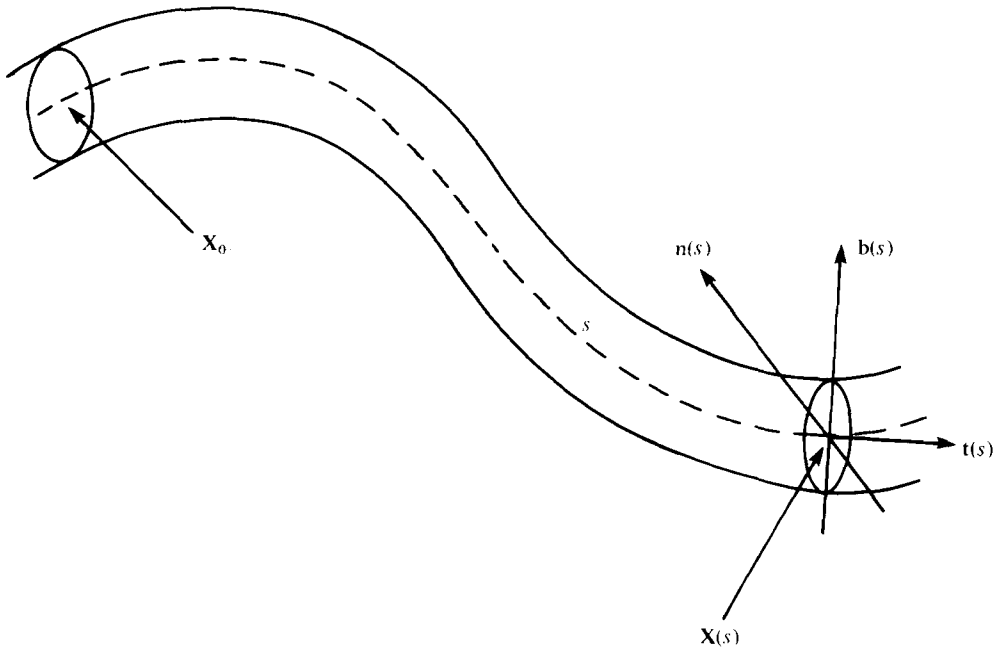

FIGURE 8. Co-ordinate system for a smooth vortex tube.

the core radius is R_0, which is constant and very much less than $R(s)$ for all s. Then a point $\mathbf{x}$ within V may be parameterized by s, r and ϕ, such that

$$\mathbf{x} = \mathbf{X}(s) + r\cos\phi\,\mathbf{n}(s) + r\sin\phi\,\mathbf{b}(s), \tag{A 2}$$

where

$$\mathbf{X}(s) = \mathbf{X}_0 + \int_0^s \mathbf{t}(s')\,ds' \tag{A 3}$$

is a point on the centre-line of the vortex loop. The radius and azimuthal position on a cross-section of the loop are respectively r and ϕ.

For any non-singular function $\mathbf{f}(\mathbf{x})$, we can therefore change variables in the integral of $\mathbf{f}$ over V, namely,

$$\iiint_V \mathbf{f}(\mathbf{x})\,d^3x = \int_0^\Sigma ds \int_0^{R_0} dr \int_0^{2\pi} d\phi\, r\left(1+\frac{r}{R(s)}\cos\phi\right)\mathbf{f}(\mathbf{x}(s,r,\phi)); \tag{A 4}$$

since $R_0 \ll R(s)$, provided that $|\nabla\mathbf{f}| = o(r^{-1}|\mathbf{f}|)$, we can write

$$\iiint_V \mathbf{f}(\mathbf{x})\,d^3x \approx \pi R_0^2 \int_0^\Sigma \bar{\mathbf{f}}(\mathbf{X}(s))\,ds, \tag{A 5}$$

where $\bar{\mathbf{f}}$ represents a suitably defined average value of $\mathbf{f}$ over the cross-section of the ring at s. Now in the case of (A 1), $\boldsymbol{\omega}(\mathbf{x}) = \omega(r)\,\mathbf{t}(s)$ and the circulation κ is given by

$$\kappa = \int_0^{R_0} 2\pi r\omega(r)\,dr. \tag{A 6}$$

With the change of variable in (A 4) and (A 5) we can rewrite (A 1) as

$$\mathbf{u}_i(\mathbf{x}') \approx -\frac{\kappa}{4\pi}\oint \frac{(\mathbf{x}'-\mathbf{X}(s))\wedge\mathbf{t}(s)}{|\mathbf{x}'-\mathbf{X}(s)|^3}\,ds, \tag{A 7}$$

provided that $\mathbf{x}' \notin V$, and neglecting terms $O(R_0/R)^2$. The evaluation of the induced velocity field far from the core of the vortex is achieved simply by calculation of (A 7); if greater accuracy is required the exact formula (A 5) may be used.

If $\mathbf{x}'$ is in V, then the integral (A 5) is essentially singular; it may be reduced to a line integral as in (A 7) away from the singularity. Without loss of generality, we define the origin of s to consider the velocity induced at $\mathbf{X}_0$. Then

$$\mathbf{u}_i(\mathbf{X}_0) \approx -\frac{\kappa}{4\pi}\int_L^{\Sigma-L} \frac{(\mathbf{X}_0-\mathbf{X}(s))\wedge\mathbf{t}(s)}{|\mathbf{X}_0-\mathbf{X}(s)|^3}\,ds - \frac{1}{4\pi}\iiint_{VL}\frac{(\mathbf{X}_0-\mathbf{x})\wedge\boldsymbol{\omega}(\mathbf{x})}{|\mathbf{X}_0-\mathbf{x}|^3}\,d^3x. \tag{A 8}$$

The cut-off length L is chosen to make the second integral as small as possible, so that $\mathbf{u}_i(\mathbf{X}_0)$ is given approximately by the first, which may be evaluated either exactly or numerically, and which need not concern us further. V_L is the section of the vortex for which $|s| < L$.

Widnall & Sullivan (1973) have used asymptotic expansions to find the value of the second integral. As a result of evaluation of (A 8) they find the expression

$$\mathbf{u}_i(\mathbf{X}_0) = \frac{\kappa}{4\pi R(0)}\,[\mathbf{B}-\mathbf{b}(s)\log_e(L/R(0))], \tag{A 9}$$

while from the equations satisfied within the vortex core they find

$$\mathbf{u}_i(\mathbf{X}_0) = \frac{\kappa}{4\pi R(0)}\left[\mathbf{B}-\mathbf{b}(s)\left(\log_e\frac{R_0}{2R(0)}+\tfrac{1}{2}-\bar{A}\right)\right]. \tag{A 10}$$

In both formulae $\mathbf{B}$ is the same $O(1)$ expression corresponding to the effect of the distant portion of the ring. $\bar{A}$ is a constant depending upon the vorticity distribution in the core;

$$\bar{A} = \frac{4\pi^2}{\kappa^2}\int_0^{R_0} r^{-1}\Gamma^2(r)\,dr, \tag{A 11}$$

where

$$\Gamma(r) = \int_0^r r'\omega(r')\,dr'; \tag{A 12}$$

$2\pi\Gamma(r)$ is the total circulation within the region of the core of radius r. In the usual case of constant vorticity, $\bar{A} = \frac{1}{4}$. A hollow-cored vortex has $\bar{A} = 0$, and $\omega \propto r^{-1}$ implies that $\bar{A} = \frac{1}{2}$. By comparing (A 9) and (A 10) we see that the first integral in (A 8) will give the value of the induced velocity at $\mathbf{x}_0$ if we choose

$$L = \tfrac{1}{2}R_0\exp(\tfrac{1}{2}-\bar{A}),$$

independent of $R(0)$.

Of a number of closed-form expressions for the kinetic energy, the most useful is that given by Lamb [1932, art. 153, equation (5)], which can be written

$$E = \frac{\rho}{8\pi}\iiint_V\iiint_{V'}\frac{\boldsymbol{\omega}(\mathbf{x})\,.\,\boldsymbol{\omega}(\mathbf{x}')}{|\mathbf{x}-\mathbf{x}'|}\,d^3x\,d^3x'. \tag{A 13}$$

The inner integral always has a singularity. Once again we introduce a cut-off length L', and write

$$E = E_1 + E_2, \tag{A 14}$$

where the portion E_1 of the integral away from the singularity can be written

$$E_1 \approx \frac{\rho\kappa^2}{8\pi}\oint ds\left\{\int_{s+L'}^{s+\Sigma-L'}\frac{\mathbf{t}(s)\,.\,\mathbf{t}(s')}{|\mathbf{X}(s)-\mathbf{X}(s')|}\,ds'\right\} \tag{A 15}$$

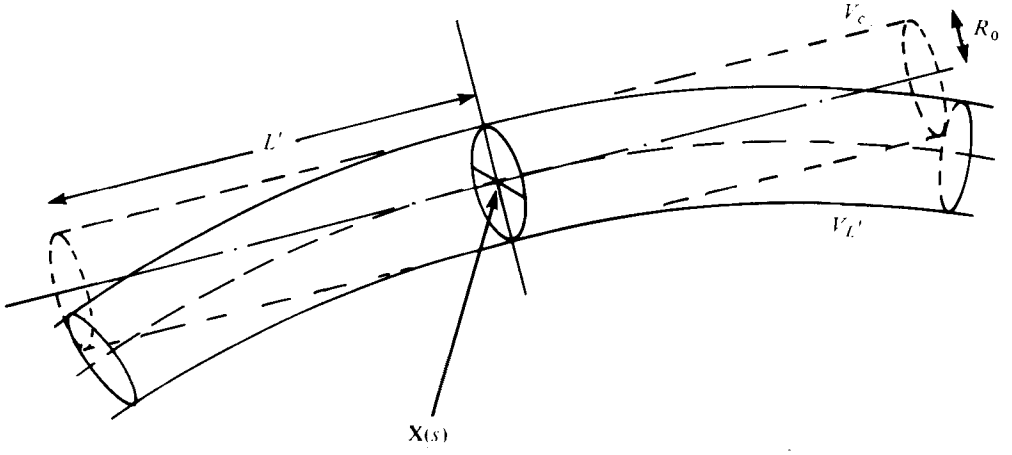

FIGURE 9. Relation of tangential cylindrical tube V_c to length of portion of curved vortex tube $V_{L'}$.

as in (A 7), since the cross-sectional radius of the vortex loop is small; the remaining portion E_2 is then

$$E_2 = \frac{\rho}{8\pi} \iiint_V \left\{ \iiint_{V_{L'}} \frac{\boldsymbol{\omega}(\mathbf{x}) \cdot \boldsymbol{\omega}(\mathbf{x}')}{|\mathbf{x}-\mathbf{x}'|} \, d^3x' \right\} d^3x, \tag{A 16}$$

where $V_{L'}$ is the section of the loop in which $|s'-s| < L'$. E_1 can be evaluated either exactly or numerically.

Since all vorticity in the core is azimuthal, we can write

$$E_2 = \frac{\rho}{8\pi} \iiint_V \omega(r)\, g(\mathbf{x})\, d^3x, \tag{A 17}$$

where

$$g(\mathbf{x}) = \iiint_{V_{L'}} \frac{\mathbf{t}(s) \cdot \mathbf{t}(s')\, \omega(r')}{|\mathbf{x}-\mathbf{x}'|} \, d^3x'. \tag{A 18}$$

We now approximate $V_{L'}$ by a circular cylinder V_c of length $2L'$ and radius R_0 tangential to the vortex at $\mathbf{x}' = \mathbf{X}$ (figure 9). Then $\mathbf{t}(s') = \mathbf{t}(s)$, so that

$$g(\mathbf{x}) = \iiint_{V_c} \frac{\omega(r')}{|\mathbf{x}-\mathbf{x}'|} \, d^3x' (1 + O(L^2/R^2)). \tag{A 19}$$

Now this is the gravitational potential at $\mathbf{x}$ of the cylinder V_c, with density $\boldsymbol{\omega}(r')$. Therefore $g(\mathbf{x})$ will satisfy

$$\nabla^2 g(\mathbf{x}) = -4\pi\omega(r). \tag{A 20}$$

We can deduce from (A 20) that $g(\mathbf{x})$ is a function of r alone; also we require values of g only on the plane through $\mathbf{X}(s)$. We can evaluate $g(0)$ from the Green's function of the Laplacian operator to find

$$g(0) = 2\pi \int_0^{R_0} r'\omega(r') \left\{ \int_{-L'}^{L'} \frac{dl'}{(l'^2 + r'^2)^{\frac{1}{2}}} \right\} dr' \tag{A 21}$$

$$\approx 4\pi \int_0^{R_0} r'\omega(r') \log_e \left(\frac{2L'}{r'} \right) dr' \tag{A 22}$$

$$= 2\kappa \log_e \left(\frac{2L'}{R_0} \right) + 4\pi \int_0^{R_0} r'^{-1} \Gamma(r')\, dr', \tag{A 23}$$

on integrating by parts. But (A 20) becomes

$$\frac{d^2g}{dr^2}+\frac{1}{r}\frac{dg}{dr} = -4\pi\omega(r), \tag{A 24}$$

so that

$$g(r) \approx 2\kappa \log_e\left(\frac{2L'}{R_0}\right)+4\pi\int_0^R r'^{-1}\Gamma(r')\,dr'. \tag{A 25}$$

By substituting into (A 17),

$$E_2 \approx \frac{\rho}{8\pi}\iiint_V \omega(r)\,g(r)\,r\left(1+\frac{r}{R(s)}\cos\phi\right)ds\,dr\,d\phi \tag{A 26}$$

$$\approx \tfrac{1}{4}\rho\Sigma\int_0^{R_0} r\omega(r)\,g(r)\,dr \tag{A 27}$$

$$= \frac{\rho\kappa^2\Sigma}{4\pi}\left(\log_e\left(\frac{2L'}{R_0}\right)+\bar{A}\right), \tag{A 28}$$

where $\bar{A}$ is as specified above and Σ is the circumference of the loop.

Therefore E_2 can be made small compared with E_1 if we choose $L' = \frac{1}{2}R_0e^{-\bar{A}}$. Then $E = E_1$, given by (A 15), will give the kinetic energy.

It is purely a question of straightforward algebra to calculate the induced velocity and kinetic energy when the vortex ring is circular. The first integral in (A 8) gives

$$\mathbf{u}_i = \frac{\kappa\mathbf{b}}{4\pi R}\left[\log_e\frac{8R}{R_0}+\bar{A}-\tfrac{1}{2}\right]; \tag{A 29}$$

the self-induced convection velocity of a circular vortex ring is constant around the circumference of the ring. The kinetic energy from (A 15) is

$$\mathrm{KE} = \tfrac{1}{2}\rho\kappa^2R\left[\log_e\frac{8R}{R_0}+\bar{A}-2\right]. \tag{A 30}$$

Both (A 29) and (A 30) are of course the familiar classical results, therefore we may have confidence in the arguments used to derive the cut-off lengths.

Similar calculations can be performed for other shapes of vortex loop. We are especially interested in the plane elliptical vortex ring; suppose the major and minor axes are of lengths 2α and 2β. The eccentricity e is given by $\beta^2 = \alpha^2(1-e^2)$ and the eccentric angle is Φ, so that a point $\mathbf{X}(\Phi)$ on the centre-line of the vortex core is given by $(\alpha\cos\Phi, \beta\sin\Phi, 0)$ in Cartesian co-ordinates with origin at the centre of the ellipse and chosen such that $\mathbf{b}$ lies along the z axis; the local radius of curvature is

$$R(\Phi) = \alpha^2(1-e^2\cos^2\Phi)^{\frac{3}{2}}/\beta.$$

Then after a good deal of algebra which is not repeated here, we find that

$$\mathbf{u}_i(\Phi) = \frac{\kappa\mathbf{b}}{4\pi R(\Phi)}\left\{\log_e\frac{8R(\Phi)}{R_0}+\bar{A}-\tfrac{1}{2}+\frac{e^2}{1-e^2}\left(e^2\cos^2\Phi-\cos 2\Phi\right)\right\} \tag{A 31}$$

and that

$$\mathrm{KE} = \frac{1}{\pi}\rho\kappa^2\alpha\left[-(1-\tfrac{1}{2}e^2)\,K(e)+E(e)\left\{\log_e\frac{8(\alpha\beta)^{\frac{1}{2}}}{R_0}+\bar{A}-1\right\}\right], \tag{A 32}$$

where $E(e)$ and $K(e)$ are complete elliptic functions of the first and second kinds. We can show from (A 31) that a useful estimate for $\mathbf{u}_i$, valid to within 10% for

$e \lesssim 0{\cdot}5$, is the self-induced velocity of the circular ring of the same impulse (same area) as the elliptic ring:

$$\mathbf{u}_i = \frac{\kappa \mathbf{b}}{4\pi(\alpha\beta)^{\frac{1}{2}}} \left\{ \log_e \frac{8(\alpha\beta)^{\frac{1}{2}}}{R_0} + \bar{A} - \tfrac{1}{2} \right\}. \tag{A 33}$$

Confidence can be felt in the expressions (A 31) and (A 32) for $\mathbf{u}_i$ and KE for the elliptic ring, for as $e \to 0$ they approach the expressions (A 29) and (A 30) for a circular ring. The expression (A 31) for $\mathbf{u}_i(\Phi)$ is not constant around the circumference of the ellipse, although it is everywhere normal to the plane of the ellipse. Therefore an elliptic vortex ring cannot retain its shape as it travels, in the way that an isolated circular ring can, but will deform and ultimately become unstable and lose its regular shape. Provided that the eccentricity e is small (less than say 0·5) the rate of deformation is small compared with the translation velocity, and (A 33) is a valuable estimate for the motion of the loop. Strictly, (A 33) can describe the local induced velocity only at the instant when the ring is generated.

The author wishes to thank all those who have offered help and advice during the course of this work, in particular Sir James Lighthill, Dr K. E. Machin, Dr T. J. Pedley and Dr C. J. Pennycuick, and also acknowledges the financial assistance of the Science Research Council.

REFERENCES

Bilo, D. 1971 Flugbiophysik von Kleinvögeln. I. Kinematik und Aerodynamik des Flügelabschlages beim Haussperling (*Passer domesticus*). *Z. vergl. Physiol.* **71**, 382–454.

Bilo, D. 1972 Flugbiophysik von Kleinvögeln. II. Kinematik und Aerodynamik des Flügelaufschlages beim Haussperling (*Passer domesticus*). *Z. vergl. Physiol.* **76**, 426–437.

Brown, R. H. J. 1963 The flight of birds. *Biol. Rev.* **38**, 460–489.

Cone, C. D. 1968 The aerodynamics of flapping birdflight. *Spec. Sci. Rep. Va Inst. Mar. Sci.* no. 52.

Csicsáky, M. J. 1977 Body-gliding in the zebra finch. *Fortschr. Zool.* **24**, 275–286.

Ellington, C. P. 1978 The aerodynamics of normal hovering flight. In *Comparative Physiology – Water, Ions and Fluid Mechanics* (ed. K. Schmidt-Nielsen, L. Bolis & S. H. P. Maddrell), pp. 327–345. Cambridge University Press.

Fraenkel, L. E. 1970 On steady vortex rings of small cross-section in an ideal fluid. *Proc. Roy. Soc.* A **316**, 29–62.

Fraenkel, L. E. 1972 Examples of steady vortex rings of small cross-section in an ideal fluid. *J. Fluid Mech.* **51**, 119–135.

George, J. C. & Berger, A. J. 1966 *Avian Myology*. Academic Press.

Greenewalt, C. H. 1962 Dimensional relationships for flying animals. *Smithson. Misc. Collns* **144**, 2.

Greenewalt, C. H. 1975 The flight of birds. *Trans. Am. Phil. Soc.* **65**, 4.

Hummel, D. & Möllenstädt, W. 1977 On the calculation of the aerodynamic forces acting on a house sparrow (*Passer domesticus*) during downstroke by means of aerodynamic theory. *Fortschr. Zool.* **24**, 235–256.

Lamb, H. 1932 *Hydrodynamics*. Cambridge University Press.

Lighthill, M. J. 1973 On the Weis-Fogh mechanism of lift generation. *J. Fluid Mech.* **60**, 1–17.

Lighthill, M. J. 1974 Aerodynamic aspects of animal flight. *5th Fluid Sci. Lecture, Brit. Hydromech. Res. Ass.* (Also in *Mathematical biofluiddynamics*. Philadelphia: SIAM, 1975.)

Magnan, A., Perrilliat-Botonet, C. & Girard, H. 1938 Essais d'enregistrements cinématographiques simultanées dans trois directions perpendiculaires deux á deux de l'écoulement de l'air autour d'un oiseau en vol. *C. r. hebd. Séanc. Acad. Sci. Paris* **206**, 462–464.

NACHTIGALL, W. 1974 Biophysik des Tierflugs. *Rheinisch-Westfälische Akad. Wissenschaften, Vorträge* **236**, 73–152.

NACHTIGALL, W. & KEMPF, B. 1971 Vergleichende Untersuchungen zur flugbiologischen Funktion des Daumenfittichs (*Alula spuria*) bei Vögeln. *Z. vergl. Physiol.* **71**, 326–341.

NORBERG, U. M. 1975 Hovering flight in the pied flycatcher (*Ficedula hypoleuca*). In *Swimming and Flying in Nature* (ed. T. Y. Wu, C. J. Brokaw & C. Brennen), vol. 2, pp. 869–881. Plenum.

NORBERG, U. M. 1976*a* Aerodynamics, kinematics and energetics of horizontal flight in the long-eared bat *Plecotus auritus*. *J. Exp. Biol.* **65**, 459–470.

NORBERG, U. M. 1976*b* Aerodynamics of hovering flight in the long-eared bat *Plecotus auritus*. *J. Exp. Biol.* **65**, 459–470.

NORBURY, J. 1973 A family of steady vortex rings. *J. Fluid Mech.* **57**, 417–431.

OEHME, H. 1968 Der Flug des Mauerseglers (*Apus apus*). *Biol. Zbl.* **88**, 287–311.

OEHME, H., DATHE, H. H. & KITZLER, U. 1977 Research on biophysics and physiology of bird flight. IV. Flight energetics in birds. *Fortschr. Zool.* **24**, 257–273.

OEHME, H. & KITZLER, U. 1974 Untersuchungen zur Flugbiophysik und Flugphysiologie der Vögel. I. Über die Kinematik des Flügelschlages beim unbeschleunigten Horizontalflug. *Zool. Jb. Physiol.* **78**, 461–512.

OEHME, H. & KITZLER, U. 1975*a* Untersuchungen zur Flugbiophysik und Flugphysiologie der Vögel. II. Zur Geometrie des Vögelflügels. *Zool. Jb. Physiol.* **79**, 402–424.

OEHME, H. & KITZLER, U. 1975*b* Untersuchungen zur Flugbiophysik und Flugphysiologie der Vögel. III. Die Bestimmung der Muskelleistung beim Kraftflug der Vögel aus kinematischen und morphologischen Daten. *Zool. Jb. Physiol.* **79**, 425–458.

OSBORNE, M. F. M. 1951 Aerodynamics of flapping flight with applications to insects. *J. Exp. Biol.* **28**, 221–245.

PENNYCUICK, C. J. 1968 Power requirements for horizontal flight in the pigeon *Columba livia*. *J. Exp. Biol.* **49**, 527–555.

PENNYCUICK, C. J. 1969 The mechanics of bird migration. *Ibis* **111**, 525–556.

PENNYCUICK, C. J. 1975 Mechanics of flight. In *Avian Biology*, vol. 5 (ed. D. S. Farnell, J. R. King & K. C. Parkes), pp. 1–75. London: Academic Press.

PENNYCUICK, C. J. & LOCK, A. 1976 Elastic energy storage in primary feather shafts. *J. Exp. Biol.* **64**, 677–689.

SPILLMAN, J. 1979 The use of wing tip sails to reduce vortex drag. *J. R. Aero. Soc.* (in the press).

RAYNER, J. M. V. 1977 The intermittent flight of birds. In *Scale Effects in Animal Locomotion* (ed. T. J. Pedley), pp. 437–443. Academic Press.

RAYNER, J. M. V. 1979*a* A vortex theory of animal flight. Part 1. The vortex wake of a hovering animal. *J. Fluid Mech.* **91**, 705–738.

RAYNER, J. M. V. 1979*b* A new theory of animal flight mechanics. *J. Exp. Biol.* (in the press).

RÜPPELL, G. 1977 *Bird Flight*. Van Nostrand Rheinhold.

SAFFMAN, P. G. 1970 The velocity of viscous vortex rings. *SIAM J.* **49**, 371–380.

TUCKER, V. A. 1972 Metabolism during flight in the laughing gull *Larus atricilla*. *Am. J. Physiol.* **222**, 237–245.

TUCKER, V. A. 1973 Bird metabolism during flight: evaluation of a theory. *J. Exp. Biol.* **58**, 689–709.

VINOGRADOV, I. N. 1951 *Aerodinamika ptits-paritelei*. Moscow: DOSARM (in Russian). (Trans. *The Aerodynamics of Soaring Bird Flight. Roy. Aircraft Establ. Trans.* no. 846, 1960.)

WEIS-FOGH, T. 1972 Energetics of hovering flight in hummingbirds and *Drosophila*. *J. Exp. Biol.* **56**, 79–104.

WEIS-FOGH, T. 1973 Quick estimates of flight fitness in hovering animals, including novel mechanisms for lift production. *J. Exp. Biol.* **59**, 169–230.

WIDNALL, S. E., BLISS, D. B. & ZALAY, A. 1971 Theoretical and experimental study of the stability of a vortex pair. In *Aircraft Wake Turbulence and its Detection* (ed. J. H. Olsen, A. Goldburg & M. Rogers), pp. 305–338. Plenum.

WIDNALL, S. E. & SULLIVAN, J. P. 1973 On the stability of vortex rings. *Proc. Roy. Soc.* A **332**, 335–353.

Note added in proof (20 February 1979)

Some recent experiments by Professor N. V. Kokshaysky have used simple flow-visualization techniques based on a cloud of fine particles to investigate the wake left by flying passerines (mainly finches). These experiments clearly demonstrate the presence of closed vortex loops, each generated by a single winged stroke, very much as predicted in §§ 1 and 3 of this paper, and discussed in greater detail in Rayner (1979*b*). Cross-sectional photographs of the wake display a vortex structure very similar to that shown diagrammatically in figure 3 (also figure 4 of Rayner 1979*b*). The experiments are not sufficiently developed to permit measurement of the size and strength of the vortex elements, but they do provide effective confirmation of the supposition made in this work that the wake must comprise a chain of small-cored smooth vortex loops.

REFERENCE

KOKSHAYSKY, N. V. 1979. Tracing the wake of a flying bird. (Submitted for publication in *Nature*.)